

THERMAL CHEMISTRY PATHWAYS OF 1-NAPHTHOL

R. H. Schlosberg and A. Kurs

Exxon Research and Engineering Company
Route 22 East, Clinton Township
Annandale, New Jersey 08801

Previously we have reported our investigations of the thermal chemistry pathways of a number of ether systems under coal conversion like conditions. (1-4). In our studies on naphthalene methyl ether pyrolysis (4), we distinguished three major reaction pathways at 400°C (750°F): O-C alkyl cleavage yielding naphthols and R-H after hydrogen abstraction, an isomerization pathway of the starting ethers and a rearrangement pathway involving initial alkyl C-H hydrogen abstraction. Cleavage of the O-C bond is the most important pathway in this system.

We showed that the decomposition kinetics of the 1-naphthalene methyl ether was faster than that of the 2-isomer and that both naphthalene ethers were thermally more reactive than anisole (Table I). The product slates for the ethers are listed in Table II.

Figure 1 depicts four possible pathways to form naphthalene from 1-naphthalene methyl ether. One way which appeared particularly attractive was hydrodeoxygenation of naphthol. In this study we pursue that question by investigating the high temperature chemistry of 1-naphthol under coal conversion like conditions.

1-Naphthol was heated to 450°C (840°F) in a 30 cc batch autoclave under an initial room temperature pressure of 500 psi (3.5 MPa) of hydrogen. At reaction temperatures, the total pressure of the system rose to ~1000 psi. As shown in Figure 2, under our (largely) gas phase reaction conditions, the major products are naphthalene and tetralin. Other products identified included 1-tetralone and 1-tetralol. The presence of these two C₁₀ oxygenates is consistent with the results of Poutsma and Dyer (5) who studied the thermal chemistry of 1-naphthol without any external hydrogen. Their work was carried out at 400°C (750°F), a temperature where 1-naphthol exists largely in the liquid phase. In their hydrogen starved system, only a 2% yield of naphthalene was obtained, comparable to our naphthalene yields from the thermolysis of the naphthalene methyl ethers (Table II).

Figure 2 shows that the yield of the hydroaromatic, tetralin, diminishes with time while that of naphthalene grows as a function of time. This is consistent with a continuing hydrogen demand from unreacted naphthol and other hydrogen deficient systems (i.e., radicals, 1-tetralone and 1-tetralol) slowly dehydrogenating tetralin to naphthalene.

Under thermal conditions where Poutsma and Dyer (5) show about 33% conversion, the major products are dinaphthylfuran (53%), 1-tetralone (18%), tetralin (3%) and naphthalene (2%). Under hydrogen at similar levels of conversion (39%), we found tetralin (35%), naphthalene (28%), and 1-tetralone (10%), with only 5% dimeric and higher molecular weight species. Clearly with moderate pressure hydrogen, even without any added catalyst, the dimerization

or "growth" pathway so damaging to high oil yields from coal pyrolyses is superseded by reduction of the hydroxyl-containing ring. We calculate a rate constant for the disappearance of 1-naphthol to be $2.2 \times 10^{-3} \text{ sec}^{-1}$ at 450°C under hydrogen and $1.3 \times 10^{-4} \text{ sec}^{-1}$ at 400°C without added hydrogen.

Scheme I provides a series of thermal steps which can account for the initial generation of phenolics, then aromatics, and finally hydroaromatics under moderate hydrogen pressure. We begin with aryl alkyl ethers, moieties determined to be important reactive components in lignins (6) and in low rank coals (7). In contrast, when the naphthol is generated without external sources of hydrogen, the dominant pathway is one of condensation to make a dimeric furan (5). Since in a coal system, there will be some available hydrogen (native to the coal) even a pyrolysis will lead to the formation of some aromatic and hydroaromatic compounds as secondary reaction products following the initial ether cleavage pathway to phenols.

Experimental

1-Naphthol (Aldrich) was used as received (capillary gc analysis showed a purity >99%). The six batch reactors employed were constructed of 316 stainless steel and have previously been described in detail (8). Each reactor was charged with 2.0g of 1-naphthol and 500 psi (3.5 MPa) of hydrogen, attached to a rack and together plunged into a preheated fluidized sand bath and moderately agitated. Heatup times are on the order of 1.5 minutes. Individual reactors were removed from the hot sand bath at various times and rapidly quenched by plunging them into a water bath. Product analysis was by capillary gc. Use of an external standard (n-hexadecane) permitted identification of >90% by weight of the charged material.

Summary

1-Naphthol thermolysis was studied at 450°C (840°F) under moderate hydrogen pressure of ~1000 psi at reaction temperatures. The surprising result is the marked difference from earlier results reported on thermolysis of 1-naphthol under nitrogen: whereas the condensed products, dinaphthylfuran and 1-tetralone are dominant under nitrogen; in the hydrogen case tetralin and naphthalene are the most important products. This change in reaction product is accounted for by a new, competitive reaction pathway provided to the system by the molecular hydrogen.

References

1. R. H. Schlosberg, T. R. Ashe, R. J. Pancirov, and M. Donaldson, *FUEL*, **60**, 155 (1981).
2. R. H. Schlosberg, W. H. Davis, Jr., and T. R. Ashe, *Ibid.*, 201.
3. R. H. Schlosberg, P. F. Szajowski, G. D. Dupre, J. A. Danik, A. Kurs, T. R. Ashe, and W. N. Olmstead, *Ibid.*, **63**, 690 (1983).
4. R. H. Schlosberg, G. D. Dupre, A. Kurs, P. F. Szajowski, T. R. Ashe and R. J. Pancirov, *Liq. Fuels Tech.*, **1**, 115 (1983).
5. M. L. Poutsma and C. W. Dyer, *J. Org. Chem.*, **47**, 3367 (1982).
6. See, e.g., K. Freudenberg, *Ann. Rev. Biochem.*, **8**, 88 (1983).
7. R. Liotta, *J. Amer. Chem. Soc.*, **103**, 1735 (1981).
8. R. C. Neavel, *FUEL*, **55**, 237 (1976).

Table I
 UNIMOLECULAR DECOMPOSITION RATES
 FOR METHYL ARYL ETHERS

Batch Autoclaves, 3.5 MPa N₂, 0.1 Hr Residence Time

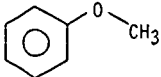
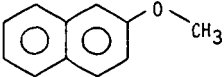
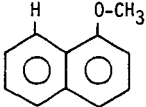
Ether		% Recovered Ether @ T=0.1 Hr <u>450°C</u>	k(hr ⁻¹)	
			<u>400°C</u>	<u>450°C</u>
	Anisole	91	-	0.94
	2-Methoxy- Naphthalene	71±2	0.5	4.1
	1-Methoxy- Naphthalene	33±3	1.4	12

Table II

NAPHTHYL METHYL ETHER PYROLYSIS RESULTS

Batch Autoclave, 0.1 Hr. Residence Time, N₂

% in Liquids by GC Analysis

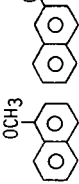
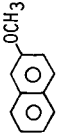
Reactant	Temperature (°C)								
	400	tr	89 ± 2	-	3 ± 1	-	1 ± 0.3	-	0.6 ± 0.2
	450	4	33	13	5 ± 1	tr	3	-	12
	400	-	-	96 ± 2	-	0.2 ± 0.1	-	-	-
	450	3	9	71	0.2	1	-	2	tr

Figure 1

POSSIBLE PATHWAYS TO NAPHTHALENE

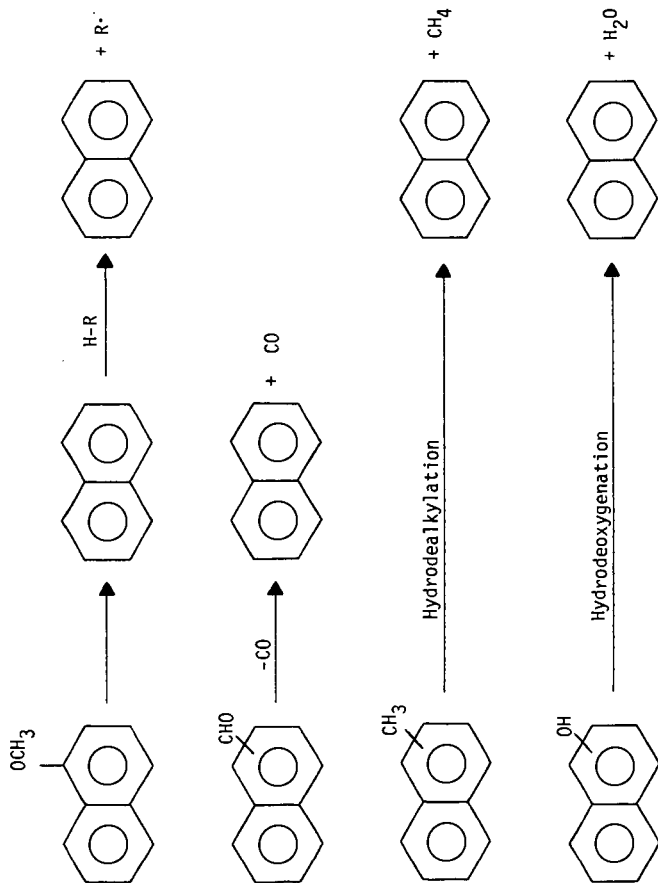
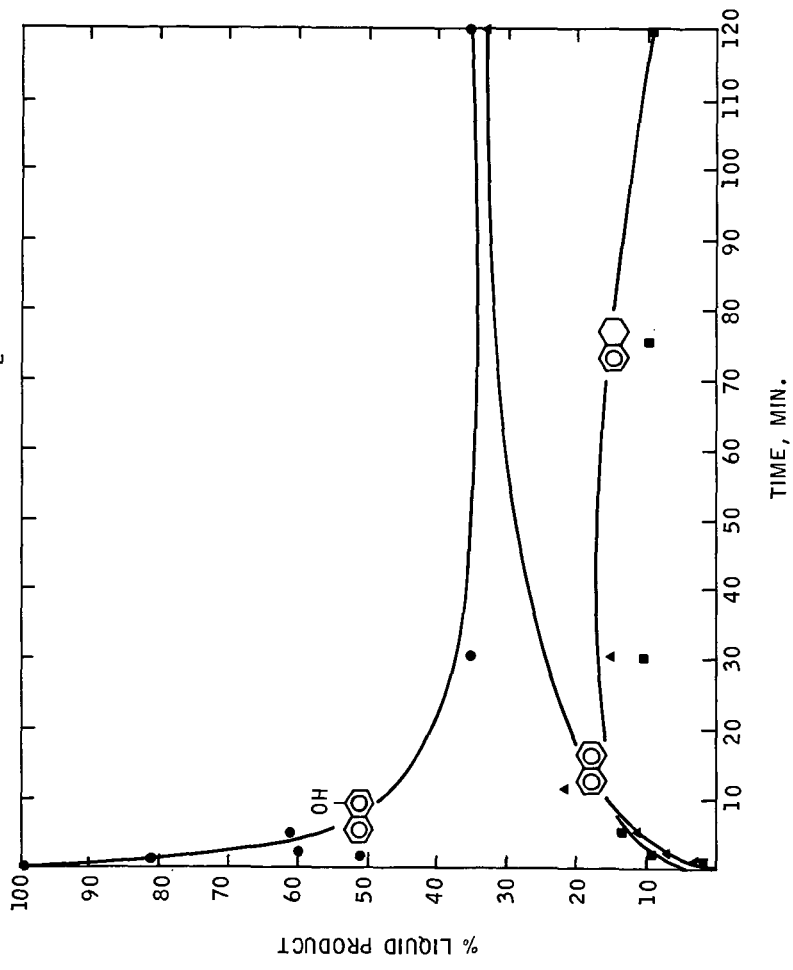


Figure 2

α -NAPHTHOL CONVERSION
450°C./500 psi H₂



THERMOLYSIS OF SUBSTITUTED ANISOLES

Antti I. Vuori and Johan B-son Bredenberg
Department of Chemistry
Helsinki University of Technology
SF-02150 Espoo 15, Finland

INTRODUCTION

The possibility of using biomass as a chemical feedstock has in recent years attracted increasing interest. Lignin is one of the major components of biomass. It is produced in large amounts during wood pulping but the main part of it is simply burnt. There should, however, be some possibilities to use part of the lignin as raw material for more valuable products (1-3).

The first reaction step in any chemical conversion process of lignin is thermal rupture to smaller units (3, 4). Only the products thus formed are small enough to react with a heterogeneous catalyst to the ultimate products. This behavior corresponds to that found for coal. Thermal reactions of lignin as well as coal are usually very complicated. This makes the interpretation of experimental results from thermal reactions of lignin quite difficult though not impossible (5-7). Study of suitable lignin related model compounds can be of great use in the interpretation of the results. Application of the results of model compound studies on more complicated structures must, however, always be done with care since the reactions of macromolecular structures are not necessarily well represented by simple model compounds as has been noted in connection with coal (8).

Thermolysis of hydroxy, methoxy and methyl substituted anisoles in the presence of tetralin has earlier been studied by Bredenberg and Ceylan (9). Their results are, however, probably influenced by effects caused by the reactor walls. This paper considers the thermolysis of the guaiacyl structure of lignin by comparing the thermal reactions of different hydroxy and methoxyanisoles (and anisole) both neat and in the presence of tetralin at molar ratio 1:1 under conditions where wall effects have been minimized. Some comments about the kinetic parameters of the model compounds studied are also made though the experiments performed are insufficient for a strict kinetic analysis.

EXPERIMENTAL

All the model compounds used as well as tetralin were pure or analytical grade and they were used without further purification. Only the meta substituted compounds contained so much impurities (about 2.5 % by GC) that these had to be accounted for in the results.

The experiments were performed in 1 ml boron silicate glass ampoules (Duran 50) under argon atmosphere as described elsewhere (10). The same analytical procedures were also followed. The GC-MS analyses were needed only for the products from the experiments with meta compounds.

In addition to the thermolysis experiments some additional experiments were performed to test the effects of different kinds of materials as well as the possible wall effect on the thermolysis of hydroxyanisoles in the presence of tetralin at 638 K. The materials used for this purpose with all three hydroxyanisoles were sodium glass, AISI 304 and AISI 316 steels, molybdenum powder, and boron silicate glass. Coal ash and silicon carbide were tested only with *o*- and *p*-hydroxyanisole. The reaction time was 3.0 h for *ortho* and *para* compounds and 5.0 h for *meta* compound. The surface

area was approximately doubled in the experiments, except for the experiments with coal ash where the area was more than two hundred times the original. The results showed that sodium glass led to the formation of higher products with all hydroxyanisoles. Molybdenum and coal ash were found to enhance the conversion of the ortho and para compounds while there was no clear trend with the meta compound. No significant difference between the runs with plain boron silicate ampoules and those where boron silicate, silicon carbide or the aforementioned steels had been added were found. It should, however, be noted that molybdenum containing steel alloys have been reported to be activated in hydroliquefaction of coal when treated with pyrocatechol (11, 12).

RESULTS AND DISCUSSION

Table 1 summarizes the experiments performed. The results are summarized in Figures 1 and 2 which contain the conversions and the selectivities of the formation of the main products from each model compound. Formation of higher products and char is also indicated in Figures 1 and 2.

All hydroxyanisoles gave as the main primary products the correspondingly substituted dihydroxybenzenes and cresols (Figure 1). Neat *m*-hydroxyanisole showed also some formation of methyl-*m*-hydroxyanisoles but because of the low conversions as well as the content of impurities (about 0.7 % methyl-*m*-hydroxyanisoles by GC) these results are uncertain. Figure 2 shows that the *o*- and *p*-methoxyanisoles followed a reaction pattern of same type as the hydroxyanisoles while *m*-methoxyanisole showed a stronger trend than *m*-hydroxyanisole to the formation of ring methylated products with two oxygen atoms. The possible pathways for product formation will be discussed in detail in relation to the C-O bonds reacting.

The methyl C-O bond

The bond energy of the methyl C-O bond in a guaiacyl structure has been evaluated to be about 247 kJ/mol (3). It is clearly the weakest bond in *o*-hydroxyanisole (guaiacol). The results in Figures 1 and 2 also demonstrate that the majority of the main products from both hydroxy and methoxy-anisoles were formed by breaking of this bond.

Breaking of this bond in all hydroxyanisoles seemed to follow two parallel primary pathways. The formation of pyrocatechol from guaiacol has earlier been explained to take place by a free radical mechanism (13) or by a concerted mechanism (14). A concerted mechanism for the formation of the corresponding dihydroxybenzenes cannot be visualized for *m*- and *p*-hydroxyanisoles.

The question of a concerted versus a free radical mechanism has been widely discussed in the context of both biomass and coal liquefaction. Stein (15) has commented on the mechanistic possibilities of the thermal reactions of guaiacol by noting that there are under conditions of very low pressure pyrolysis where bimolecular reactions cannot occur, methyl radicals but little or no methane as a product. This would indicate a free radical reaction. The mechanism of guaiacol thermolysis is obviously more complicated under high concentration. The presence of water, which is formed during the reaction, has also been found to have a pronounced effect on the thermolysis of guaiacol (16). A combined free radical chain and concerted mechanism has recently been proposed for thermolysis of dibenzyl ether in the presence of tetralin (17).

Our results (Table 2) showed that the rate of decomposition of guaiacol was about one order of magnitude higher than that of any other model compound studied. The apparent first order activation energy found for guaiacol in the presence of tetralin (Table 3) was also unusually low which is in agreement with the values reported elsewhere (14). This

suggests that in addition to the homolytic mechanism an additional reaction mechanism, i.e. the concerted mechanism is also operating. It is in this connection important to note that o-methoxyanisole did not show any similar trend.

The formation of correspondingly substituted cresols from the hydroxyanisoles as well as the formation of correspondingly substituted cresols and methylanisoles from o- and p-methoxyanisoles was the second primary pathway of the methyl C-O bond cleavage. For the para compounds an intramolecular ipso-substitution seems to be the only reasonable explanation. For the ortho and meta compounds an intermolecular methylation is still possible though, especially for the meta compound hardly probable. For the ortho compounds there is, in addition, the possibility of an intramolecular methyl shift to the ortho position from the methoxyl group. Ceylan and Bredenberg (13) have presented an intramolecular rearrangement of guaiacol to o-cresol which takes place via an enolic form of the ortho hydroxyl. No significant interaction between the substituents in m-hydroxyanisole can be expected. Therefore the ipso-substitution requires some other mechanism. Anisole has been explained to react through a phenoxymethyl radical formed by methyl hydrogen abstraction to a benzyloxy radical via a spiranic oxiran intermediate under corresponding reaction conditions (10, 18). The primary products from a benzyloxy radical are, however, benzaldehyde and benzyl alcohol which in turn can then be reduced to toluene. There was no indication of this type of products in any GC or GC-MS analyses made of the thermolysis products of hydroxy and methoxyanisoles during the present work. It should, however, be noted that Kisilitsyn et al. (19) have found both o-hydroxybenzaldehyde and o-hydroxybenzyl alcohol among the products of short contact time pyrolysis of guaiacol at 773 K.

The results of the experiments with m-methoxyanisole (Figure 2) differed from those noted above. The cleavage of the methyl C-O bond to form m-hydroxyanisole corresponds

to the reaction of the other compounds studied. There was, however, no noticeable ipso-substitution of the methyl group despite of the greater proportion of ring methylated dihydroxy compounds. m-Hydroxyanisole also showed a similar trend. This is probably due to the ortho-para-activating effect of both hydroxyl and methoxyl groups. The meta compound has been found to give the greatest proportion of ring methylated products also in catalytic hydrodeoxygenation of hydroxyanisoles (20).

It is also interesting to note that the decomposition rate of neat m-methoxyanisole was roughly twice the decomposition rate of neat anisole (Table 2). This could be interpreted to mean that the methoxyl groups in m-methoxyanisole react fairly independently.

The aromatic C-O bond

The bond energy of the aromatic C-O bond of the methoxyl group in a guaiacyl structure has been evaluated to be about 356 kJ/mol, and of the hydroxyl group about 414 kJ/mol (3). For the corresponding homolytic bond scissions a high activation energy is hence required. This correlates well with the fact that guaiacylic model compounds have usually been found to give, under mild thermolysis conditions, only small amounts of products with one oxygen atom (6, 13, 14, 21).

Our results suggest that there was no significant direct scission of the aromatic C-O bonds in guaiacol (Figure 1). The formation of phenol takes place most probably via pyrocatechol. The results of the experiments with m- and p-hydroxyanisole are not as clear.

Anisole and aromatic hydrocarbons were found only in trace amounts in the hydroxyanisole series. The scission of the phenolic C-O bond has been suggested by Stein (15) to take place probably by an ionic mechanism. Tentative experiments

performed with the dihydroxybenzenes in the presence of tetralin gave almost exclusively phenol as a single ring aromatic product from pyrocatechol and hydroquinone whereas no phenol was found in experiments with resorcinol. These experiments also showed that higher products were formed from hydroquinone even in the presence of tetralin, a result which can also be seen in Figure 1.

The results of the methoxyanisole series (Figure 2) showed significant differences in the breaking of the aromatic C-O bonds in comparison with the hydroxyanisole series. In addition to the formation of phenol there was also significant formation of anisole from all three methoxyanisoles. The analyses made also indicated the presence of the products formed in the decomposition of anisole (10).

Anisole has earlier been reported to be formed from *o*-methoxyanisole (22). The formation of anisole from all three methoxyanisoles is not easily explained. It must take place by direct demethoxylation but the presence of a hydroxyl group seems to prevent it for reasons not known.

The overall kinetics

The decomposition rates of all the model compounds studied can be fitted into first order kinetics (Table 2) though the gross conversion include parallel reaction pathways. The apparent first order activation energies are shown in Table 3. These values are partly uncertain since in some cases they are based only on a few experiments at two temperatures (Table 1). Hence, only a few comments are made. The unusually low activation energy of guaiacol in the presence of tetralin has already been discussed. The results of neat guaiacol are too few for a proper analysis. Tables 2 and 3 also show that tetralin has, in addition to decreasing the reaction rates, some effect on the apparent activation energies. This is probably due to the quenching effect tetralin has on free radical chain reactions.

CONCLUSIONS

The main reaction in the thermolysis of all hydroxyanisoles is the breaking of the methyl C-O bond. Two reaction pathways can be distinguished, the first one leading to the formation of the correspondingly substituted dihydroxybenzenes, and the second one leading to the formation of the correspondingly substituted cresols. For guaiacol the former pathway takes partly place, in addition to a homolytic bond breaking, by a concerted mechanism. A concerted mechanism cannot, however, be visualized for *m*- and *p*-hydroxyanisole. The latter pathway is thought to take place via a spiranic oxiran intermediate. For guaiacol there is also the possibility of an intramolecular methyl shift to the ortho position from the methoxyl group. The formation of cresols via methyl-dihydroxybenzenes does not, however, seem to be very probable. Neat *m*-hydroxyanisole shows, in addition, some formation of methyl-*m*-hydroxyanisoles. Breaking of the aromatic C-O bond in the hydroxyanisoles occurs only to a minor extent under mild thermolysis conditions.

The *o*- and *p*-methoxyanisoles follow a reaction pattern of the same type as the hydroxyanisoles while *m*-methoxyanisole gives more ring methylated products with two oxygen atoms. There is, however, no indication of a concerted mechanism for *o*-methoxyanisole. The formation of anisole by direct demethoxylation is significant for all three methoxyanisoles.

The decomposition rate of all the model compounds studied is decreased by the presence of tetralin.

ACKNOWLEDGEMENTS

This work has been funded in part by grants from the Ministry of Education and Neste OY Foundation. The authors are grateful to Mrs. Eija Kinnunen and Mr. Timo Karinen for their contribution to the experimental part of this work.

REFERENCES

1. Deglise, X. and Lede, J., *Int Chem.Eng.* 22 (1982), 631-646.
2. Kringstad, K., The challenge of lignin, in *Future sources of organic raw materials - CHEMRAWN I*, ed. by St-Pierre, L.E. and Brown, G.R., Pergamon Press, Oxford etc. 1980, 627-636.
3. Parkhurst, H.J., Jr., Huibers, D.T.A. and Jones, M.W., *Prepr.Pap. ACS Div. Pet.Chem.* 25 (1980), 657-667.
4. Avni, E., Coughlin, R.W., Solomon, P.R. and King, H.H., *Prepr.Pap. ACS Div. Fuel Chem.* 28 (1983), no.5, 307-318.
5. Iatridis, B. and Gavalas, R., *Ind.Eng.Chem.Prod.Res.Dev.* 18 (1979), 127-130.
6. Connors, W.J., Johanson, L.N., Sarkanen, K.V. and Winslow, P., *Holzforsch.* 34 (1980), 29-37.
7. Jegers, H.E. and Klein, M.T., paper submitted to *Ind. Eng.Chem.Process Des.Dev.*
8. McMillen, D.F., Ogier, W.C. and Ross, D.S., *Proc. - Int.Kohlenwiss.Tag, Essen 1981*, 104-109.
9. Bredenberg, J.B. and Ceylan, R., *Fuel* 62 (1983), 342-344.
10. Vuori, A., Karinen, T. and Bredenberg, J.B., *Finn.Chem. Lett.* 1984, in print.
11. Yoshii, T., Yaginuma, R., Yoshikawa, H. and Utoh, S., *Fuel* 61 (1982), 865-866.
12. Yoshii, T., Yaginuma, R., Utoh, S. and Yoshikawa, H., *Fuel* 62 (1983), 47-49.
13. Ceylan, R. and Bredenberg, J.B., *Fuel* 61 (1982), 377-382.
14. Klein, M.T. and Virk, P.S., *Prepr.Pap. ACS Div.Fuel Chem.* 25 (1980), no.4, 180-190.
15. Stein, S.E., *ACS Symp.Ser.* 1981, no.169, 97-129.
16. Lawson, J.R. and Klein, M.T., paper submitted to *Ind. Eng.Chem.Fundam.*
17. Simmons, M.B. and Klein, M.T., paper submitted to *Ind. Eng.Chem.Fundam.*
18. Schlosberg, R.H., Szajowski, P.F., Dupre, G.D., Danik, J.A., Kurs, A., Ashe, T.R. and Olmstead, W.N., *Fuel* 62 (1983), 690-694.
19. Kislitsyn, A.N., Rodionova, Z.M., Savinykh, V.I., Il'ina, E.I. and Abakhumov, G.A., *Sb.Tr.Tsent.Nauch.-Issled. Proekt.Inst.Lesokhim.Prom.* 1971, no.22, 4-16.

20. Bredenberg, J.B., Huuska, M. and Toropainen, P., Proc. 9th Iberoam.Symp.Cat., Lisboa 1984, Vol. I, 650-657.
21. Vuori, A. and Bredenberg, J.B., Holzforsch. 38 (1984), 133-140.
22. Klein, M.T. and Virk, P.S., Report MIT-EL 81-005, 1981, 99 p.

Table 1. Experimental data.

model compound	reaction temperature (K)	reaction time (h)
<i>o</i> -OH-anisole, neat	623	0.6; 1.0; (2.0)
	648	0.5; 1.0; 2.0; 3.0
	673	(1.0; 2.0)
-with tetralin	623	0.75; 1.0; 2.0; 3.0; 4.0
	648	0.5; 0.5; 1.0; 2.0; 2.0; 3.0; 4.0; 4.0
<i>m</i> -OH-anisole, neat	623	2.0; 3.0; 4.0
	648	1.0; 1.0; 2.0; 2.0; 3.0; 4.0
	673	1.0; 1.0; 2.0; 4.0; 4.0
-with tetralin	648	0.5; 1.0; 2.0; 3.0; 4.0; 4.0
	673	0.5; 1.0; 2.0; 2.0; 3.0; 4.0
<i>p</i> -OH-anisole, neat	648	1.0; 2.0; 4.0
	673	0.5; 2.0
-with tetralin	648	0.5; 1.0; 2.0; 2.0; 3.0; 4.0; 4.0
	673	0.5; 1.0; 2.0; 2.0; 3.0; 4.0
<i>o</i> -OCH ₃ -anisole, neat	648	1.0; 2.0; 4.0
	673	0.25; 0.5; 2.0
-with tetralin	623	1.33; 2.0; 4.0; 5.0; 7.0
	648	1.0; 1.0; 2.0; 3.0; 4.0
	673	0.5; 1.0; 1.0; 1.5; 2.0
<i>m</i> -OCH ₃ -anisole, neat	623	2.0; 3.0; 4.0
	648	1.0; 1.0; 2.0; 4.0
	673	1.0; 2.0; 2.0; 4.0
-with tetralin	648	1.0; 2.0; 2.0; 3.0; 4.0
	673	0.5; 1.0; 1.5; 2.0; 2.0
<i>p</i> -OCH ₃ -anisole, neat	648	1.0; 2.0; 4.0
	673	0.25; 0.5; 2.0
-with tetralin	623	1.33; 2.0; 4.0; 5.0; 7.0
	648	1.0; 1.0; 2.0; 3.0; 4.0
	673	0.5; 1.0; 1.0; 1.5; 2.0

-experiments in parentheses are not used for kinetic parameters.

Table 2. The apparent first order rate coefficients of the model compounds.

model compound	623 K		648 K		673 K	
	$10^5 k$ (1/s)	r	$10^5 k$ (1/s)	r	$10^5 k$ (1/s)	r
-neat						
anisole(10)						
o-OH	12.5 \pm 1.0	0.997	0.76 \pm 0.13	0.959	3.91 \pm 0.59	0.957
m-OH	0.43 \pm 0.02	0.998	1.34 \pm 0.11	0.983	23.7 \pm 2.6	0.977
p-OH			5.36 \pm 0.83	0.977	54.0 \pm 9.4	0.985
o-OCH ₃			7.41 \pm 1.05	0.981	70.8 \pm 14.2	0.962
m-OCH ₃	0.51 \pm 0.13	0.945	1.33 \pm 0.16	0.979	8.09 \pm 1.67	0.942
p-OCH ₃			6.84 \pm 0.75	0.988	57.0 \pm 14.4	0.942
-with tetralin						
anisole(10)						
o-OH	6.58 \pm 0.39	0.993	0.31 \pm 0.04	0.967	2.09 \pm 0.16	0.987
m-OH			23.0 \pm 1.4	0.987		
p-OH			0.48 \pm 0.11	0.897	1.93 \pm 0.14	0.986
o-OCH ₃	1.52 \pm 0.11	0.989	2.50 \pm 0.16	0.988	18.5 \pm 1.0	0.992
m-OCH ₃			8.01 \pm 0.73	0.984	45.7 \pm 2.4	0.995
p-OCH ₃	1.02 \pm 0.12	0.975	1.00 \pm 0.19	0.932	4.58 \pm 0.20	0.996
			5.82 \pm 0.54	0.983	30.3 \pm 0.4	1.000

Table 3. The apparent first order Arrhenius parameters of the model compounds.

model compound	E_A (kJ/mol)	$\log_{10} A$ (1/s)
-neat		
anisole(10)		
o-OH	237 \pm 46	14.0 \pm 3.7
m-OH	143 \pm 20	8.1 \pm 1.7
p-OH	277 \pm 11	17.8 \pm 0.9
o-OCH ₃	335 \pm 49	22.7 \pm 3.9
m-OCH ₃	327 \pm 51	22.3 \pm 4.1
p-OCH ₃	192 \pm 31	10.7 \pm 2.5
	308 \pm 57	20.6 \pm 4.6
-with tetralin		
anisole(10)		
o-OH	276 \pm 30	16.8 \pm 2.3
m-OH	168 \pm 16	9.9 \pm 1.3
p-OH	201 \pm 40	10.9 \pm 3.1
o-OCH ₃	290 \pm 17	18.8 \pm 1.4
m-OCH ₃	237 \pm 9	15.0 \pm 0.7
p-OCH ₃	221 \pm 32	12.8 \pm 2.5
	237 \pm 9	14.8 \pm 0.6

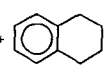
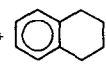
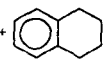
 <p>623 K, 0.6-2.0 h X = 25.8-40.8 % 648 K, 0.5-3.0 h X = 52.3-98.0 % 673 K, 1.0-2.0 h X = 99+ %</p>	<p>HIGHER, 623 K- CHAR, 648 K-</p>      <p>S (%) : 14.7-15.8 4.3-6.6 2.7-3.1 1.4-1.6 1.0-1.3 S (%) : 7.1-18.2 1.2-5.2 3.0-4.1 0.6-1.5 0.5-1.1 S (%) : 4.4-8.5 1.0-1.6 6.5-8.8 0.4-0.6 0.4-0.6</p>
<p>+</p>  <p>623 K, 0.75-4.0 h X = 14.4-60.0 % 648 K, 0.5-4.0 h X = 25.1-96.8 %</p>	     <p>S (%) : 71.7-82.0 2.4-7.7 2.7-4.9 6.0-8.1 6.0-7.0 S (%) : 64.1-83.6 3.6-10.3 2.0-14.3 4.4-7.2 3.8-5.2</p>
 <p>(97.5%) 623 K, 2.0-4.0 h X = 3.4-6.1 % 648 K, 1.0-4.0 h X = 3.6-17.5 % 673 K, 1.0-4.0 h X = 41.7-97.5 %</p>	<p>HIGHER, 648 K- CHAR, 673 K-</p>      <p>S (%) : 34.6-44.9 6.6-12.4 5.9-7.3 27.5-30.2 3.0-5.1 S (%) : 42.7-67.1 2.8-5.1 1.3-13.4 17.7-27.9 2.5-5.2 S (%) : 0.7-23.1 1.8-5.0 0.3-1.5 0.3-6.0 0.3-2.0</p>
<p>+</p>  <p>648 K, 0.5-4.0 h X = 0-8.4 % 673 K, 0.5-4.0 h X = 3.3-24.7 %</p>	     <p>S (%) : 24.7-64.2 - - - 4.9-14.7 S (%) : 56.7-86.6 8.5-16.3 - - 10.1-15.4</p>
 <p>648 K, OH 1-4 h X = 26.3-54.7 % 673 K, 0.5-2.0 h X = 81.0-98.3 %</p>	<p>HIGHER, 648 K- CHAR, 673 K-</p>      <p>S (%) : 26.6-27.9 8.4-10.6 4.0-5.9 1.7-2.7 S (%) : 5.8-24.3 4.4-7.2 7.1-8.3 0.8-2.1</p>
<p>+</p>  <p>648 K, 0.5-4.0 h X = 4.0-31.1 % 673 K, 0.5-4.0 h X = 26.4-93.7 %</p>	<p>HIGHER, 673 K-</p>      <p>S (%) : 63.4-82.2 8.4-12.1 1.4-2.4 8.2-9.4 S (%) : 30.7-78.5 10.7-12.2 2.1-3.6 5.3-7.2</p>

Figure 1. Main products from the experiments with hydroxy-anisoles.

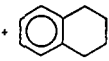
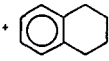
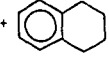
 648 K, 1.0-4.0 h X = 36.5-67.1 % 673 K, 0.25-2.0 h X = 84.7-99.7 %	CHAR, 648 K-      
	S (%) : 14.0-18.8 1.9-5.4 3.1-4.9 0.6-3.4 5.6-7.5 9.8-11.8 S (%) : 0.2-7.2 4.7-11.2 4.0-4.5 4.1-6.6 0.6-2.6 4.6-9.1
+  623 K, 1.33-7.0 h X = 5.7-30.5 % 648 K, 1.0-4.0 h X = 17.2-69.8 % 673 K, 0.5-2.0 h X = 55.3-96.3 %	     
	S (%) : 34.7-63.8 10.4-22.8 2.3-8.1 7.4-15.4 1.6-4.5 5.4-15.0 S (%) : 13.7-55.8 6.3-47.0 2.8-7.3 0.7-1.7 9.5-14.4 4.6-7.9 S (%) : 2.0-19.5 46.3-58.3 2.5-6.9 1.3-4.0 8.3-11.4 4.9-9.3
 (97.5%) 623 K, 2.0-4.0 h X = 5.8-7.2 % 648 K, 1.0-4.0 h X = 5.6-17.8 % 673 K, 1.0-4.0 h X = 41.4-70.2 %	HIGHER, 673 K-     
	S (%) : 26.0-32.2 30.2-34.8 2.4-7.4 - 9.3-11.6 S (%) : 34.9-39.6 22.7-32.2 4.8-8.2 - 11.5-16.6 S (%) : 16.6-29.6 1.9-11.4 2.9-5.7 1.3-4.0 17.8-20.5
+  648 K, 1.0-4.0 h X = 3.5-14.6 % 673 K, 0.5-2.0 h X = 10.9-28.9 %	    
	S (%) : 36.7-58.9 12.8-21.0 12.1-14.7 2.7-5.3 8.5-23.2 S (%) : 44.2-55.1 9.4-15.6 6.4-11.9 1.8-3.8 14.6-21.7
 648 K, 1.0-4.0 h X = 26.7-62.9 % 673 K, 0.25-2.0 h X = 87.1-99.2 %	HIGHER, 648 K- CHAR, 673 K-      
	S (%) : 16.1-23.0 0.5-0.6 0.8-1.5 0.3-0.6 8.8-10.1 10.8-14.6 S (%) : 3.3-15.4 4.6-4.8 2.3-5.1 2.5-5.8 2.9-6.1 6.6-15.8
+  623 K, 1.33-7.0 h X = 3.1-21.2 % 648 K, 1.0-4.0 h X = 13.7-58.6 % 673 K, 0.5-2.0 h X = 43.7-88.9 %	     
	S (%) : 61.7-73.1 2.2-3.4 (2.0) 6.0-10.9 4.2-6.7 8.8-11.2 S (%) : 57.7-68.4 2.1-10.6 1.0-3.9 0.8-1.7 9.0-11.5 4.2-9.7 S (%) : 40.1-66.1 7.2-26.0 1.7-7.1 1.2-1.6 9.3-9.8 8.0-10.8

Figure 2. Main products from the experiments with methoxy-anisoles.

THERMAL CHEMISTRY PATHWAYS OF ESTERS AND KETONES

by

R. H. Schlosberg, A. Kurs, G. D. Dupre and R. J. Pancirov

Exxon Research and Engineering Company
Route 22 East, Clinton Township
Annandale, NJ 08801

INTRODUCTION

The work described is a continuation of our studies of the thermal chemistry pathways of reactive oxygenates important in fossil fuel hydrocarbons. Esters and ketones are pyrolysis products from carboxylic acids. Ketones have been found to be important components of hydroxyrolysis oils from low rank coals, fossil fuels known to contain substantial amounts of carboxylate functionality.

THERMAL CHEMISTRY PATHWAYS OF ESTERS

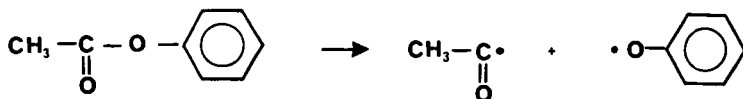
Conventional organic chemistry textbook wisdom describes ester pyrolysis only in terms of olefin elimination, and this only with esters of carboxylic acids. Noller (1) states that "when esters that have hydrogen on the β -carbon of the alkoxy group are heated to 500°C, a molecule of acid is lost with the formation of an olefin". This process is called pyrolytic cis-elimination. The situation with esters lacking β -hydrogens is less well studied and even the textbook cases are somewhat more complex than described.

Hexyl acetate. Hexyl acetate eliminates acetic acid to form 1-hexene according to the textbook mechanism, but this is not the only thermal chemistry event. Our thermal studies were carried out both in a flash pyrolysis unit (Figure 1) and in batch autoclaves. Conditions were set to achieve conversion levels of 10-60%. The thermal chemistry mechanisms are independent of unit. Using the flash pyrolysis unit and establishing a vapor residence time of ~ 1-2 sec, the major components in the gas phase products included hydrogen, methane, ethylene, propylene, water, carbon dioxide, and surprisingly carbon monoxide along with the anticipated 1-hexene (Table I). Experiments at equivalent conditions showed that acetic acid produces acetone, water and carbon dioxide as major products. Since, as we will show below, ketones thermally decarbonylate, the thermal conversion of hexyl acetate proceeds through 1-hexene and acetic acid. Acetic acid itself is thermally reactive and produces water and acetone. The ketone decarbonylates to produce the carbon monoxide observed. Finally, the 1-hexene slowly cracks and according to the results of Rebeck (2) produces C_1-C_5 products with a relatively high yield of propylene. Our results are fully consistent with this picture.

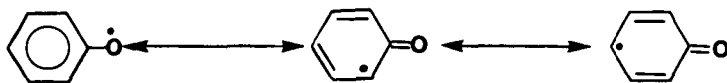
Methyl acetate. This ester does not have the structural properties required for pyrolytic cis-elimination, and at the 18% conversion level produces acetone, methanol and water as the major liquid phase products. This would indicate acyl oxygen, rather than alkyl oxygen, cleavage.

Phenyl acetate. Phenyl acetate unimolecularly decomposes only at the acyl oxygen site due to the influence of the aryl ring. As expected, the only major organic liquid products of any consequence are phenol >>> benzene. The unimolecular rate constant for phenyl acetate decomposition is 0.35 min^{-1} s. 0.44 min^{-1} for benzoic acid decomposition under similar conditions (3), (4).

A new mechanism is proposed to account for reaction products when olefin elimination is not feasible due to structural constraints. This proposed mechanism is shown in Scheme I for phenyl acetate. Cleavage at the phenolic position has been shown to be a favored pathway in the thermolysis of benzyl phenyl ether (5). ArO-H and $\text{ArCH}_2\text{-H}$ bonds are similar in strength, and



it is reasonable to invoke phenoxy radical formation in the thermal chemistry of phenyl acetate. A contributing driving force for this cleavage reaction at the benzylic position is the enhanced stability of benzyl and/or phenoxy radicals through delocalization of the free electron.

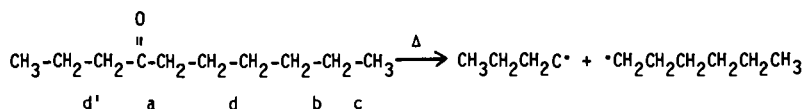


THERMAL CHEMISTRY PATHWAYS OF KETONES

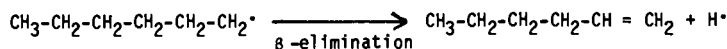
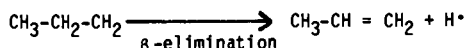
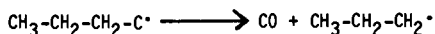
4-Decanone. Treatment of this internal ketone at 600°C in the flash pyrolysis unit led to conversion levels of 18%. The major fragmentation products (accounting for 85% of the converted ketone) were ethylene, propylene, carbon monoxide and 1-hexene (Table II). The rate constant for the unimolecular decomposition of 4-decanone was calculated to be $\sim 7.9 \text{ min}^{-1}$. This experimentally determined activation energy implies a radical chain, since there is no bond this weak ($\sim 36 \text{ kcal/mol}$) in the system. A mechanism which accounts for all of the observed products is shown in Scheme II.

SCHEME II

Initiation



Radical Elimination Reactions



Cleavage at the (b) or (c) bonds can lead to octenones and nonenones and to methane and ethane/ethylene, all identified in the product. Acetone arises from a sequence of reactions ultimately resulting in cleavage at the d and d' positions.

2-Decanone. The activation energy was calculated to be ~ 38 Kcal/mol for the unimolecular decomposition of this ketone with a rate constant at 600°C of ~11 min⁻¹. Table III presents the product data for the thermolysis of 2-decanone at 550 and 650°C. Here, as found with the 4-isomer, carbon monoxide is a significant product, thus confirming the statement made earlier that acyl radicals decompose releasing carbon monoxide. Ring closure to form aromatic rings becomes an important pathway by 650°C as does formation of solid carbonaceous material.

Aliphatic ketones are formed from the pyrolysis of carboxylic acids. They, in turn, decompose thermally to lighter olefins and acetone, and at sufficiently severe conditions to methane, carbon monoxide and coke.

1-Tetralone. A cyclic ketone such as 1-tetralone undergoes a different sequence of thermal transformations. Tetralin, naphthalene and 1-naphthol are the major liquid products when 1-tetralone is treated at 425°C under an inert atmosphere. When hydrogen is present the yields of tetralin and naphthalene increase, consistent with results published earlier (Table IV).

Acknowledgements

The authors acknowledge the support and counsel of Drs. M. L. Gorbaty and W. N. Olmstead. R. Behul is thanked for his experimental work on the 1-tetralone system.

REFERENCES

1. C. R. Noller, "Chemistry of Organic Compounds", W. B. Saunders Co., Philadelphia, 1966, p. 198.
2. C. Rebick, in "Advances in Chemistry Series. 183", American Chemical Society, 1979, p.1.
3. R. Schlosberg, manuscript submitted for publication.
4. E. Ghibandi and A. J. Colussi, J. Chem. Soc., Chem. Comm. 1984, 433 have shown that at $T > 680^{\circ}\text{C}$, phenyl acetate decomposes unimolecularly via a four-centered cyclic transition state giving phenol and ketene.
5. R. T. Morrison and R. N. Boyd, "Organic Chemistry", 2nd Edition, Allyn and Bacon, Inc., Boston, 1967, p. 688.
6. R. H. Schlosberg, W. H. Davis, Jr. and T. R. Ashe, FUEL, 60, 201 (1981).
7. S. Stein in "New Approaches in Coal Chemistry", ACS Symposium Ser. Vol. 69, Blauster, B. D., et. al., Eds., Pittsburg, PA, 1981, pp. 97-130.
8. The thermal chemistry pathways of 1-naphthol has been reported: see M. Poutsma and C. W. Dyer; J. Org. Chem., 47, 3367 (1982).
9. R. H. Schlosberg, P. F. Szajowski, G. D. Dupre, J. A. Danik, A. Kurs, T. R. Ashe and W. N. Olmstead, FUEL, 62, 690 (1983).

TABLE I
PYROLYSIS OF HEXYL ACETATE
550°C, ~1-2 SEC. RESIDENCE TIME, HELIUM SWEEP GAS

Gas Analysis, Relative Mole %

<u>H₂</u>	<u>CO</u>	<u>CO₂</u>	<u>CH₄</u>	<u>C₂H₄</u>	<u>C₂H₆</u>	<u>C₃H₆</u>	<u>C₃H₈</u>	<u>C₄'S</u>	<u>C₅'S</u>	<u>C₆'S</u>	<u>H₂O</u>
39	12	12	7.7	3.7	-	4.4	1.1	1.8	-	10	5.2

TABLE II
4-DECANONE THERMOLYSIS
600°C, ~1-2 SEC. VAPOR RESIDENCE TIME
3.8g FEED, HELIUM SWEEP GAS

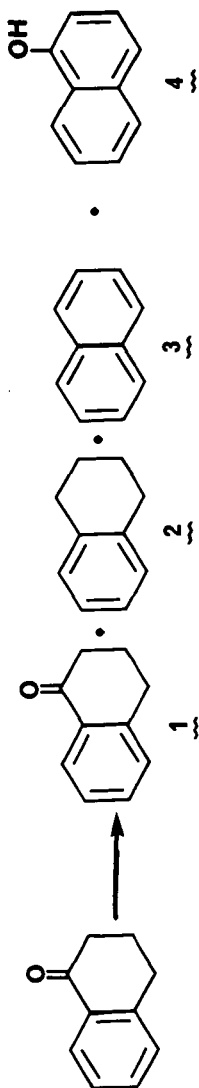
<u>Yields</u>	<u>g</u>	<u>% of Starting Feed</u>
Solid	0.02	0.53
Liquid	3.27	86.3
4-Decanone	3.11	82.1
Acetone	0.024	0.62
1-Hexene	0.049	1.3
n-Hexane	0.002	0.05
Nonenones	0.021	0.56
Others	0.064	1.7
Gases	0.48	12.7
H ₂	0.002	0.05
CH ₄	0.050	1.3
C ₂ H ₆	0.035	0.9
C ₂ H ₄	0.12	3.1
C ₃ H ₈	0.005	0.12
C ₃ H ₆	0.10	2.8
C ₄ 's	0.038	1.0
C ₅ 's	0.014	0.4
CO	0.11	2.8
H ₂ O	0.07	0.2
Total Recovered	3.77g	99.4

TABLE III
2-DECANONE PYROLYSIS
 1-2 SEC. VAPOR RESIDENCE TIME

Yields	3.73 g Feed			
	g	550°C % of Starting Feed	650°C g	% of Starting Feed
Solid	0.09	2.4	0.45	12.1
Liquid	3.67	98.4	1.81	48.5
2-decanone	3.59	96.2	1.23	33.1
acetone	-	-	0.036	1.0
1-hexene	0.003	0.07	0.039	1.1
n-hexane	-	-	0.011	0.31
2-hexenes/C ₆ H ₆	tr	tr	0.101	2.71
1-heptene	0.022	0.61	0.093	2.89
n-hexane	-	-	0.009	0.25
2-heptenes/C ₇ H ₈	-	-	0.051	1.37
1-octene	0.029	0.80	0.091	2.45
n-octane	tr	tr	0.010	0.27
2-octenes/EB,XYL	-	-	0.047	1.25
CH ₃ CO ₆ ⁼ or CH ₃ CO-cyclohexyl	tr	tr	0.015	0.40
others	0.034	0.93	0.87	2.34
Gases	0.093	2.5	0.84	22.5
H ₂	0.005	0.1	0.112	3.0
CH ₄	0.013	0.3	0.115	3.1
C ₂ H ₆	-	-	0.053	1.4
C ₂ H ₄	0.015	0.4	0.108	2.9
C ₃ H ₈	0.001	tr	0.097	2.6
C ₄ 's	0.008	0.2	0.033	0.9
C ₅ 's	0.024	0.6	0.003	0.1
CO	0.023	0.6	0.303	8.1
H ₂ O	0.004	0.1	0.009	0.2
<u>TOTAL RECOVERED</u>	3.85	103.2	3.10	83.1

TABLE IV

THERMAL CHEMISTRY OF α -TETRALONE



Reaction Atmosphere	Wt. % of Liquids			
	1	2	3	4
3 MPa He	28	19	20	25
3 MPa H ₂	8	52	29	-
5 MPa H ₂	2	56	35	-

MECHANISTIC MODELING OF THE PYROLYSIS OF ETHYLENE BRIDGED POLYMERS

K.R. Squire, P.R. Solomon, M.B. DiTaranto and R.M. Carangelo

Advanced Fuel Research, Inc., 87 Church Street, East Hartford, CT 06108, USA

Recently, Solomon and King reported a tar formation model applicable to the pyrolysis of softening bituminous coals (1). Their theory combined the random cleavage of weak bonds (similar to a concept used by Gavalas and coworkers (2)) with transport of depolymerization fragments by vaporization and diffusion (like Unger and Suuberg (3)). It predicted char and tar yields and molecular weight distributions and provided several insights into the role of donatable hydrogen and the dependence of product distributions on reaction conditions.

The Solomon and King (SK) theory was developed using model polymers which contain functional groups representative of coal structure. Polymers were studied because coal is generally insoluble, heterogeneous, and chemically complex and is, therefore, difficult to use in validating models. Several types of bridging groups between the aromatic rings in these polymers were considered; it was found that ethylene bridges decompose in the same temperature range where coal evolves tar while oxymethylene bridges cleave at temperatures which are too low and methylene bridges at temperatures which are too high (1,4,5). From these studies it's been found that ethylene bridged polymers are quite valuable in elucidating the mechanisms of tar formation since they have simple, well established chemical structures and melt and produce tars under conditions similar to those where softening bituminous coals form tar. Studies on lignins have also shown that cleavage of oxyethylene and ethylene bridges both play important roles in the formation of tar during pyrolysis of lignins (6).

Although the SK tar formation model has been found to provide reasonable predictions for tar and char yields and for the molecular weight distributions of tars, it contains three significant conceptual problems:

- 1) Reaction yields were controlled in this model by an adjustable parameter which determined how many donatable hydrogens were available for capping the arylmethylene radicals formed when ethylene bridges cleave. This parameter has been found to vary with reaction conditions and not predictable a priori.
- 2) The effect of product olefinic bridges on the bond breaking distributions was not included. The presence of unbreakable double bonds in the oligomer chains should make it less likely that monomers and dimers will form.
- 3) It is difficult to extend the SK model to include realistic chemical mechanisms since the actual concentrations of ethylene and olefinic bridges are not monitored. Attempts to correct this problem have led to excessive computer run-times.

In this paper, a revised version of the SK model is presented which can predict product yields and molecular weight distributions directly from initial polymer structures. In this model all three of these problems have been eliminated. In addition, this new model has been solved using Monte Carlo techniques, is more efficient computationally than the SK model, and can potentially be expanded to detailed simulations of extremely complex polymers such as coal. Furthermore, since this model predicts product spectra directly from polymer structures without use of adjustable parameters, it can be used to investigate the validity of alternative pyrolysis mechanisms. Simulations using this model suggest that ipso substitutions by H radicals occur during thermal decomposition of ethylene bridged polymers and that radical recombination reactions play an important role in determining the molecular weight distributions of pyrolysis tars.

EXPERIMENTAL

Poly(p-xylylene), 1, was purchased from Frinton Laboratories. As a byproduct of di-p-xylylene (p-cyclophane) synthesis, this polymer was very impure and contaminated with the dimer. It was purified by Soxhlet extraction in toluene for two days.

Poly(1,4-dimethylenenaphthalene), 2, as prepared at Iowa State University using an adaptation of Golden's synthesis for poly(dimethylenedurene) (7). This synthesis was accomplished using phenyllithium to couple the bis(bromomethyl) derivatives which were prepared from dimethylnaphthalenes using N-bromosuccinimide and benzoyl peroxide in CCl_4 . The degree of polymerization (DP), defined as the number of monomer units in a polymer molecule, is estimated to be 64 (MW = 10,000). Additional use of these polymers as models for coal chemistry was recently described by Squires et al. (8).

Several pyrolysis experiments, including slow heating rate and flash pyrolyses, were carried out on these ethylene bridged polymers using an apparatus which employs an electrically heated grid within an infrared cell to provide on-line, in-situ analysis of evolved products by Fourier Transform Infrared (FT-IR) spectrometry. Details of these experiments have been described previously (1,10). Field Ionization Mass Spectrometry (FIMS) were performed at SRI International and have been described by St. John and coworkers (11).

THEORY

The original SK tar formation model considered the molecular weight distribution, Q_i in the reacting polymer and the molecular weight distribution, N_i of the tar, where Q_i and N_i are the molar quantities of the polymeric component with $\text{DP}=i$ in the reacting polymer and in the tar. The rate of change of Q_i was written as:

$$dQ_i/dt = (dF_i/dt) - (dB_i/dt) - (dN_i/dt) \quad (1)$$

where dF_i/dt was the rate of formation for the component with $\text{DP}=i$ from the decomposition of components with $\text{DP} > i$ in the reacting polymer; dB_i/dt was the rate of disappearance by decomposition of the component with $\text{DP}=i$ in the reacting polymer; and dN_i/dt was the rate of transport of fragments with $\text{DP}=i$ from the particle as tar or gas.

The terms of dF_i/dt and dB_i/dt were the rate of creation and destruction of oligomers with $\text{DP}=i$ through the cleavage of weak bonds. The cleavage of these weak bonds was assumed to be a first order process with a rate constant k , i.e., the rate at which bonds break was k times the number of breakable bonds. It was further assumed that all bonds in a given oligomer were equivalent and were breakable. Thus, since there were $(i-1)$ bonds in the polymeric component with $\text{DP}=i$, and the breaking of any one of them would remove that component from the distribution parameter Q_i , the rate of destruction for the component i was written as

$$dB_i/dt = (i-1)kQ_i \quad (2)$$

Similar arguments were also used to write down the rate at which component i was created from oligomers with $\text{DP} = j > i$ (see Eqs. 3 and 4 of Ref. 1).

From Eqs. 1 and 2 it can be seen that this model only kept track of the molar quantities of tar and polymer oligomers; the actual concentrations of ethylene or olefinic bridges were not monitored. Instead, it was assumed that a $\text{DP}=i$ oligomer always contained $(i-1)$ breakable ethylene bridges.

Since weak ethylene bridges were not explicitly removed when they donated hydrogens to "cap" free radicals, another parameter was necessary to determine the extent of reaction. In the SK model, the extent of reaction was controlled by an adjustable parameter, F_{pqb} , defined as the fraction of weak bonds (ethylene bridges) whose resulting free radicals could be stabilized by donatable hydrogens. The total number of cleaved bonds was continuously monitored during a pyrolysis simulation and, when it

got larger than F_{pdb} , the reaction was said to have completed. Thus, F_{pdb} directly controlled char and tar yields in the original SK model. Unfortunately, this parameter varied from polymer to polymer and also depended upon reaction conditions. It could not be predicted from just a knowledge of the polymer's structure and reaction conditions.

This formulation for tar formation led to simple equations which were easy to solve and also produced reasonable predictions for tar molecular weight distributions (1,4). However, it is clearly incorrect to assume that a $DP=1$ oligomer always contains (1-1) breakable bonds, because as the depolymerization reaction proceeds, many ethylene bridges are converted to olefinic bridges following their use as hydrogen sources. Towards the end of tar formation it is entirely possible that a $DP=1$ oligomer would contain no breakable ethylene bridges. In a more realistic model the actual numbers of both olefinic and ethylenic bonds need to be monitored.

To take into account the effect of olefinic bridges it is necessary to keep track of the number of oligomers with no double bonds, with 1 double bond, with 2 double bonds, etc. This means that for each $DP=m$ oligomer, the concentrations of m double bond combinations need to be monitored. To follow the depolymerization of a polymer with initial chain length n , the concentrations of approximately $(n^3)/2$ different oligomers need to be followed. The time evolution of each of these oligomer concentrations is described by a separate differential equation. Thus, even this simple model improvement leads to a dramatic increase in the computational effort necessary to solve it! To avoid solving these complex networks of coupled differential equations, a new approach to the modeling of tar formations has been developed.

The essential problem of modeling polymer pyrolyses is simply that each modified oligomer is technically a new chemical species. As more complex oligomers are treated, the number of differential equations describing the time evolutions of these oligomers rapidly proliferates and becomes computationally unmanageable. An alternative approach is to use Monte Carlo modeling techniques.

In a Monte Carlo simulation, separate differential equations for the concentrations of individual modified oligomers are not explicitly solved. Instead, a small representative sample of polymer molecules is symbolically constructed in the memory of a computer. A bonding array is used to keep track of each monomer's identity, which substituents are attached to a given monomer, and how the monomers are connected to each other. The first four columns of this array are pointers indicating how monomers are attached to other monomers or substituents; the next four columns indicate the bonds involved in each attachment; and the last keeps track of each monomer's identity (e.g. benzene or naphthalene rings). A separate row is stored in this array for each monomer included in the simulation. Pyrolysis is simulated by statistically changing the bonding patterns stored in this array according to the kinetic and vaporization rate laws of the tar formation model.

In the current configuration, 25-40 polymer molecules can be simulated during a single run so that approximately 1200 ethylene bridges are being decomposed. Each monomer can be connected to as many as four other monomers or ring substituents. Up to fifty different monomers and twenty bond types can be used to construct the polymers for each simulation. For example, unreacted polymer 1 would be simulated using only benzene monomers, ethylene bridge connections between monomers, and methyl end groups for the terminal monomers of each polymer chain. As the pyrolysis simulation proceeded, new bond types would be introduced (e.g. olefinic bridges between monomers) to describe the gradual decomposition of the polymer.

Vaporizations are simulated by removing an oligomer from the computer's memory, by adding its mass to the running tar yield, and by putting a count in the appropriate bin of a file describing the molecular weight distribution of the evolving tar. For example, when a molecular weight 312 trimer from polymer 1 vaporizes (composition: 3 benzene monomers, 2 terminal methyl groups, 1 olefinic bridge, 1 ethylene bridge), all its pieces would be removed from the bonding arrays, 312 atomic mass units would be

added to the tar yield, and a single count would be added to bin 312 of the tar's molecular weight distribution file.

A typical simulation proceeds as follows: A series of random numbers are chosen to determine which "global" reactions occur. In the current configuration, oligomer evaporations and a complex network of reactions describing the decomposition of ethylene bridges are the "global" reactions. The random numbers are compared with normalized reaction velocities to see if the pending reaction will occur. If the random number is larger than the velocity, then the program branches to a subroutine which performs the appropriate reaction "chemistry" on the oligomer arrays. If the random number is smaller than the velocity, then the next reaction is tested until the list is exhausted. After every twenty iterations through the reaction list, time is incremented using the observed concentration changes and reaction velocities. The simulation continues until a preset time is reached or no further changes in the bonding arrays are occurring.

The reactions which have been included in the mechanism for ethylene bridge decomposition are presented in Fig. 1. In Step 1, ethylene bridges homolytically cleave to form two arylmethylene radicals. This step is assumed to be rate-limiting and its kinetic rate constants are in good agreement with predictions based upon thermochemical kinetics calculations (5).

The arylmethylene radicals can then react in six ways: they can abstract hydrogens from unreacted ethylene bridges (Step 2) or butylene bridges (Step 3), they can substitute for ethylene bridges (Step 4) or aromatic methyl groups (Step 5), and they can recombine with other arylmethylene radicals (Step 6) or with ethylene bridge radicals (Step 7). Which of these pathways occurs during a given pass through the "chemistry" subroutine is determined by comparing a random number with a set of normalized branching probabilities. In the current program fixed branching probabilities are used to determine how the decomposition proceeds, but in a future model we plan to calculate the individual velocities of the reactions in Fig. 2 using rate constants and steady state radical populations. In these simulations, branching probabilities will be the normalized ratios of these reaction rates.

Steps 2-5 lead to new radicals which continue to react while 6 and 7 produce stable bonds and terminate the reaction. The butylene bridge radicals of Step 3 are assumed to spontaneously decompose via a β -elimination reaction into an ethylene bridge radical and an olefinic bridge, Step 11. The arylethyl and methyl radicals produced in Steps 4 and 5 are assumed to stabilize via abstraction of hydrogens from unreacted ethylene bridges, Steps 15 and 16. Thus, all four of the reactive pathways for arylmethylene radicals eventually form an ethylene bridge radical.

In this model, ethylene bridge radicals are allowed to react in three ways: they can disproportionate (Step 8), they can recombine to form butylene bridges (Step 9), or they can decompose via a β -elimination reaction into a hydrogen radical and an olefinic bridge (Step 10).

The hydrogen radicals formed in Step 10 can then react in three ways: they can abstract hydrogens to stabilize (Step 12), they can substitute for ethylene bridges (Step 13), or they can substitute for aromatic methyl groups (Step 14). The arylethyl and methyl radicals formed in Steps 13 and 14 are assumed to stabilize via hydrogen abstractions from unreacted ethylene bridges, Steps 15 and 16. Thus, all the reactions of hydrogen radicals lead to the formation of new ethylene bridge radicals to replace the ones lost when Step 10 formed H radicals.

This complex network of reactions is an extension of the mechanisms proposed by Stein (12) and Poutsma (13) for the pyrolysis of diphenylethane. In the current Monte Carlo model, these reactions are carried out on the polymer bonding arrays each time the simulation determines that an ethylene bridge has decomposed. Figure 2 is a flow diagram which shows how the "chemistry" is carried out by the simulation.

as predicted by the SK model. With 90% recombination of end radicals (Fig. 5c) the increase in high molecular weight oligomer counts is sizeable, while recombinations of bridge radicals (5d) make high molecular weight oligomers less abundant.

Comparing the experimental FIMS data for polymer 1, Fig. 5a, with these simulated spectra it is apparent that even higher end radical recombination frequencies are necessary to reproduce this polymer's uneven oligomer patterns. Clearly, however, recombinations of bridge radicals can not be contributing to the observed maximum in this polymer's FIMS data.

To understand why recombinations of end radicals lead to increased populations of high molecular weight oligomers while recombinations of bridge radicals decrease their populations, we need to consider the counting statistics for each type of radical: for end radicals the probability of a radical occurring on an oligomer is independent of chain length (they occur only at the ends of chains) while for bridge radicals the probability of a radical occurring on an oligomer increases with chain length (more bridges increase the number of sites where a radical can occur).

When two end radicals recombine, oligomers can be lost in the formation of larger oligomers or they can be formed from smaller ones. For the DP = i oligomer, the terms appearing in the time derivative would be:

$$R_i = \sum_{j=1}^{i-1} f_{i-j} f_j - f_i \sum_{j=1}^a f_j \quad (3)$$

Here the f's are the probabilities of forming each radical oligomer and a is the largest oligomer which can recombine. The first term is due to formations from smaller oligomers and the second is due to losses in the formation of larger oligomers. From the SK tar model we know that roughly equal numbers of each size oligomer are formed by the homolytic bond cleavage reaction (Fig. 5b), so we conclude that f_i is, to first approximation, a constant and is independent of the degree of polymerization. Putting $f_i = c$ into equation 3 the result is:

$$R_i = c^2(i-a-1) \quad (4)$$

Thus, recombinations of end radicals decrease the rate of formation of all oligomers but they affect the time derivatives of large radicals less than those of small ones. The net effect is a shift in the tar mass spectrum towards longer chain length oligomers.

When end radicals recombine with bridge radicals, a different result is found. Now the terms appearing in the time derivative are products of the probability of finding end radicals, f's, and the probability of finding radical bridges, g's.

$$R_i = \sum_{j=1}^{i-2} g_{i-j} f_j + \sum_{j=2}^{i-1} f_{i-j} g_j - f_i \sum_{j=2}^a g_j - g_i \sum_{j=1}^a f_j \quad (5)$$

The f's are still independent of the degree of polymerization, i.e., $f_i = c$. However, the g's are proportional to the number of bridges in an oligomer or $g_i = b(i-1)$. When these probabilities are inserted in Eq. 5, the sums are slightly more difficult but can still be carried out. We find that

$$R_i = bc(i^2 - (3+a)i + 2 + a - \frac{a(a-1)}{2}) \quad (6)$$

This contribution to the time derivatives is quadratic in the degree of polymerization and reaches a minimum at $i = (a+3)/2$. For our simulations, recombinations can occur for at least 40 oligomers (the starting degree of polymerization) so this minimum occurs at a DP of at least 21. Inserting $a = 40$ and some typical values of i into this formula we find:

$$R_1 = -781 bc \quad R_5 = -928 bc \quad R_{10} = -1068 bc \quad R_{15} = -1158 bc \quad (7)$$

Thus, for recombinations between end and bridge radicals, the contributions to the

rates of formation of the oligomers with $DP < 21$ are all negative and get more negative with increasing chain length. These terms result in the formation of relatively fewer midsized oligomers when these recombinations occur than when no recombinations occur.

Similar calculations for recombinations of two bridge radicals can also be carried out and yield a cubic equation for R_1 . This cubic is negative in the range $DP = 1$ to 15 and gets more negative with increasing oligomer chain lengths. Thus, recombinations of bridge radicals also result in the formation of relatively fewer midsized oligomers during pyrolysis of these ethylene bridged polymers.

Both kinds of recombination reactions are probably important in pyrolyses of ethylene bridged polymers, lignins, and coals. The maximum in the FIMS data of polymer 1 seems to be caused by recombination of end radicals while rapid mass drop-offs are observed in the FIMS spectra of lignins (6), lignites (1), and ethylene bridged methoxybenzene polymer (5). Examples of these FIMS spectra will be presented during the talk.

ACKNOWLEDGEMENT

The authors would like to thank the Gas Research Institute for their support under contract #5081-260-0582.

REFERENCES

1. Solomon, P.R. and King, H.H., *Fuel*, **63**, 1302, (1984).
2. Gavalas, G. R., Cheong, P. H. and Jain, R. "Ind. Eng. Chem. Fundam.," **20**, 113 and 122 (1981).
3. Unger, P. E. and Suuberg, E. M. "Eighteenth Symposium (International) on Combustion", The Combustion Institute, Pittsburgh, PA, (1981), 1203.
4. Solomon, P.R., "Synthesis and Study of Polymer Models Representative of Coal Structure", Gas Research Institute Annual Report for Contract #5081-260-0582. GRI Accession #GRI-83/0171 (April, 1983).
5. Squire, K.R., Solomon, P.R., DiTaranto, M.B., "Synthesis and Study of Polymer Models Representative of Coal Structure", Gas Research Institute Annual Report for Contract #5081-260-0582. GRI Accession #GRI-84/0083 (May, 1984).
6. Squire, K.R. and Solomon, P.R., "Characterization of Biomass as a Source of Chemicals", NSF Final Report under Contract No. CPE-8107453, (1983).
7. Golden, J.H., *J. Chem. Soc.* (1961), 1604-1610.
8. Squires, T.G., Smith, B.F., Winans, R.E., Scott, R. and Hayatsu, R., "International Conference on Coal Science", Pittsburgh, PA, Proceedings, p. 292, (1983).
9. Golden, J.H., *J. Chem. Soc.* (1961), 3741-3738.
10. Solomon, P. R. and Hamblen, D. G., "Chemistry and Physics of Coal Utilization, AIP Conference Proceedings No. 70, Amer. Inst. Phys., New York (1981), pg. 121.
11. St. John, G.A., Buttrill, S.E., Jr., and Anbar, M., "Field Ionization and Field Desorption Mass Spectroscopy Applied to Coal Research, in "Organic Chemistry of Coal", (Ed. J. Larsen, ACS Symposium Series, 71, pg. 223, (1978).
12. Stein, S.E., "New Approaches in Coal Chemistry", (Ed. Blaustein, B.D., Bockrath, D.C., and Friedman, S.), Am. Chem. Soc. Symposium Ser. 169, Washington, DC, pg. 208, (1981).
13. Poutsma, M.L., *Fuel*, **59**, 335, (1980).

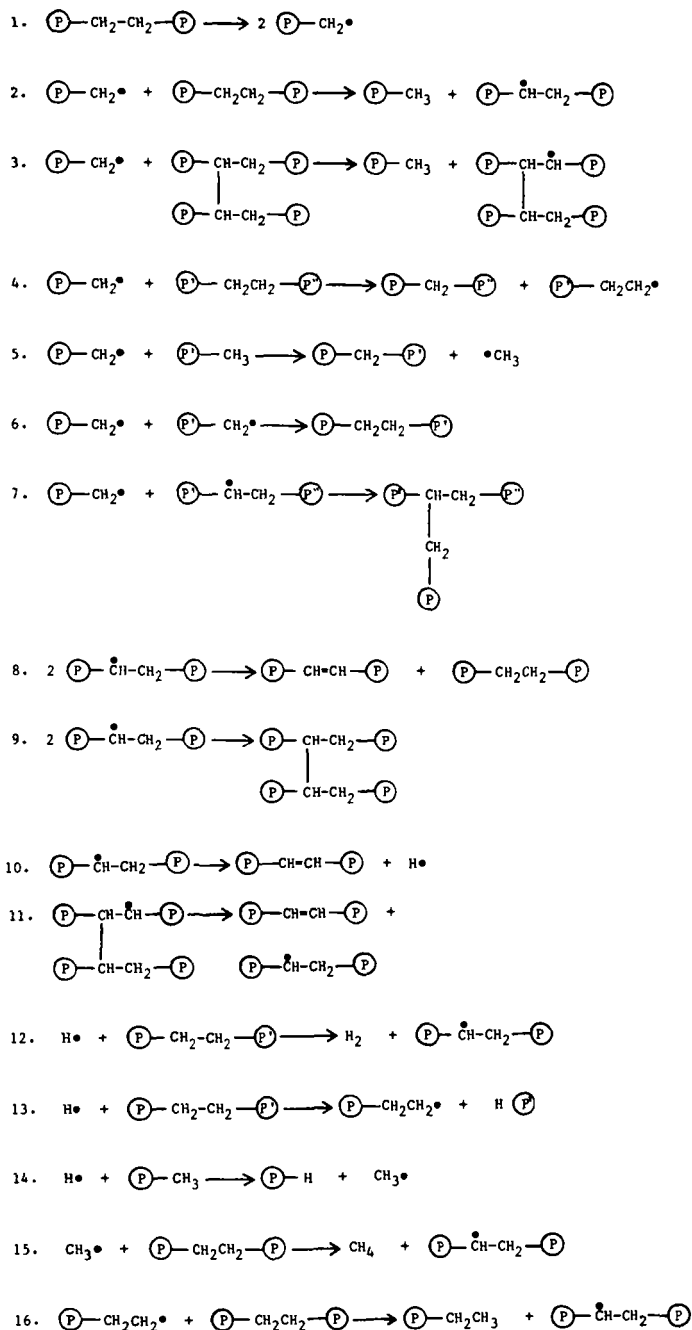


Fig. 1 Proposed Mechanism for the Decomposition of Ethylene Bridges.

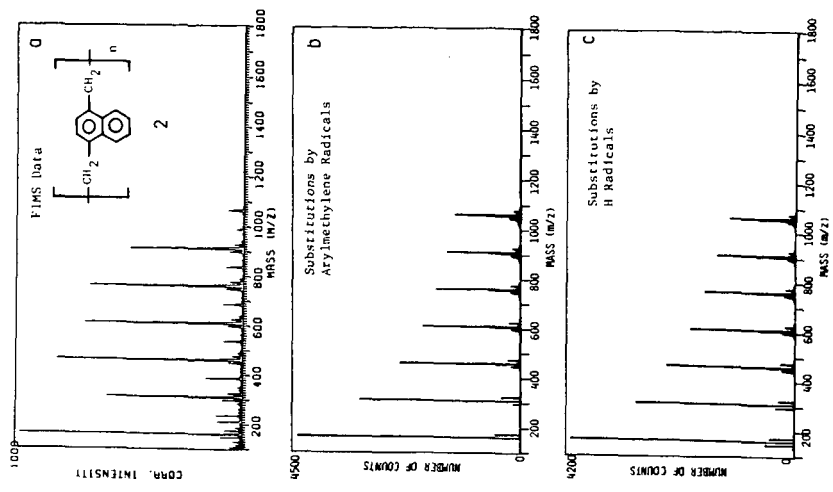


Figure 4. Monte Carlo Simulations for Polymer 2.

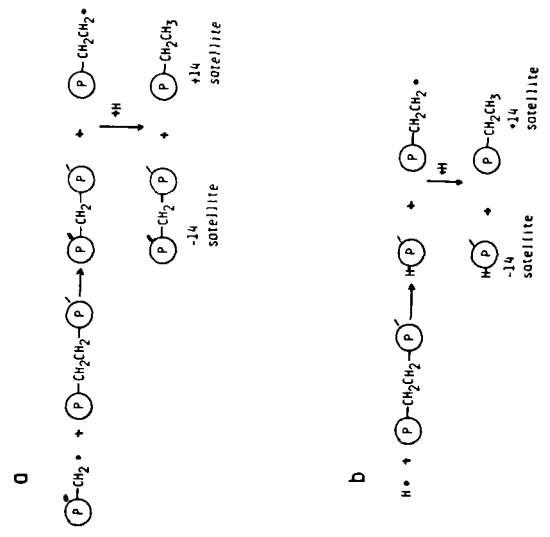


Figure 3. Mechanisms for Ipso Substitution Reactions. a) Substitutions by Arylmethylene Radicals. b) Substitutions by H Radicals.

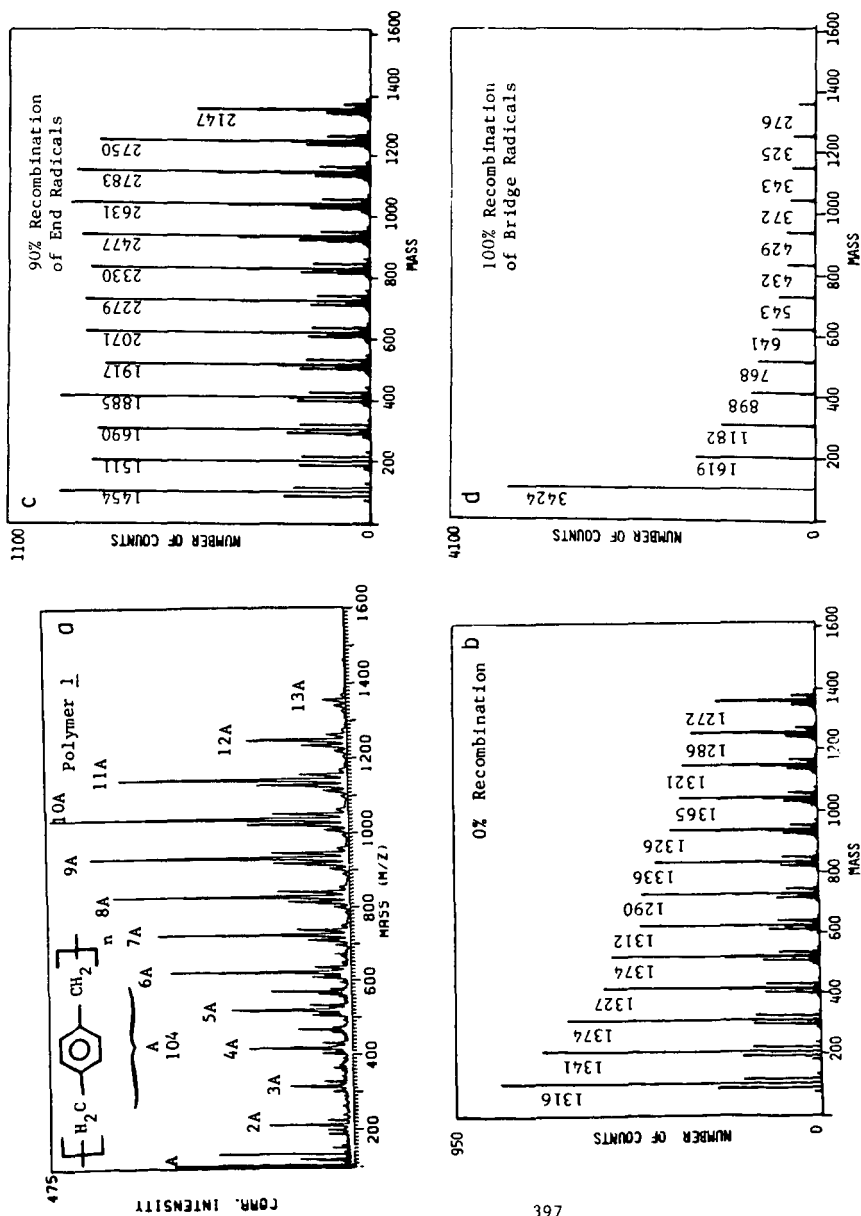


Fig. 5 Monte Carlo Simulations for Polymer 1.

SOLVENT EFFECTS DURING THE REACTION OF COAL AND
BIOMASS MODEL COMPOUNDS IN DENSE WATER

J. R. Lawson, J. R. Obst, M. A. Abraham, S. H. Townsend and M. T. Klein
University of Delaware
Department of Chemical Engineering
Newark, DE 19716

INTRODUCTION

The chemical reactions that accompany the extraction (1) of volatiles from hydrocarbon resources with supercritical water (SCW) are frequently obscured by the complexities of the reaction system. In contrast, the comparative simplicity of model compound structures and product spectra permit resolution of reaction fundamentals (2) and subsequent inference of the factors that control the reactions of real reacting systems. Herein we use model compounds to probe the kinetics of the pyrolysis and solvolysis reactions that likely occur during the extraction of volatiles from coals and lignins.

A previous study of the reaction of guaiacol (orthomethoxyphenol), a mimic of key structural aspects of lignin, in SCW (3) elucidated parallel pyrolysis and hydrolysis pathways, the selectivity to the latter increasing linearly with water density. Guaiacol decomposition kinetics were interestingly nonlinear in water density, which suggested the possibility of unusual cage or solvent effects attributable to dense fluids. We have observed qualitatively similar behavior for the reaction of each of dibenzyl ether (DBE), benzyl phenyl amine (BPA), and benzyl phenyl sulphide (BPS) in SCW and wish to report a candidate reaction network that unifies the previous and present model compound results.

RESULTS

Table I summarizes the reaction conditions of temperature, reactants' concentrations and holding time. Measured amounts of tap water and the commercially available (Aldrich) substrates DBE, BPA and BPS were entered into room temperature stainless steel "tubing bombs" that have been described elsewhere (3). Sealed reactors were immersed into a fluidized sand bath held constant at the desired reaction temperature, which was attained by the reactors in about 2 min; this heat-up period was small compared to ultimate reaction times (up to 40 min) and was, in any case, identical for all runs. Products were identified by GC-MS and quantitated by GC as described elsewhere (3,4).

Neat DBE pyrolysis led to toluene and benzaldehyde as major products along with lesser amounts of benzene and benzyl alcohol. DBE reaction in SCW gave benzyl alcohol, toluene, benzaldehyde and high molecular weight oligomers (4) as major products along with 1,2-diphenylethane, diphenylmethane and triphenylmethane as minor products. The influence of water density (S) on DBE decomposition kinetics is illustrated in Figure 1, where DBE conversion (x) is plotted against water density for parametric values of the reaction time at

374°C. Note that each curve in Figure 1 passes through a minimum value of x ; these occurred at about $S = 0.4 \pm 0.05$ in all cases.

Pyrolysis of BPA led to toluene, aniline, benzalaniline and oligomers as major products and minor products including 1,2 diphenylethane and 2-benzylaniline. BPA reaction in water was to benzyl alcohol and benzaldehyde as well as the neat pyrolysis products. The influence of S on BPA reaction kinetics at 386°C is illustrated in Figure 2. For each reaction time illustrated in Figure 2, BPA conversion passes through a minimum as water density increases.

Neat pyrolysis of BPS was to the major product toluene as well as thiophenol, phenyldisulfide, and phenylsulfide. Diphenylmethane and 1-2-diphenylethane were minor products. BPS reaction in water led to all of the neat pyrolysis products except diphenylmethane, as well as minor amounts of benzaldehyde. The influence of S on BPS reaction kinetics at 300°C is illustrated in Figure 3. For each reaction time in Figure 3, BPS conversion passes through a minimum as water density increases.

DISCUSSION

Two experimental observations common to the reaction of each of guaiacol, DBE, BPA and BPS merit summary. First, the overall reaction of each substrate in dense water comprised parallel pyrolysis and solvolysis pathways, with the selectivity to the latter increasing continuously with increasing water density. Second, and for a constant reaction temperature and time, each reactant's conversion passed through a minimum as the water density increased. These observations are consistent with the two complementary mechanistic interpretations that form the basis of the model reaction networks of Figures 4a and 4b. We consider these separately.

In the mechanism represented in Figure 4a, the general reactant R can follow either pyrolysis or solvolysis reaction paths. Neat pyrolytic fragmentation of R to product spectrum P_1 may, in general, require hydrogen consumption, which will be provided by the reactants themselves. Thus, n of Figure 4a will typically be 3, 0, 1 and 1 for guaiacol, DBE, BPA and BPS, respectively (3,5). Solvolysis to product spectrum P_2 in Figure 4a is modelled to occur through a solvated reactant intermediate, R^S , that is caged by m water molecules. Increases in water density will shift the overall observed reaction product spectrum from P_1 (pyrolysis-like) toward P_2 (solvolysis-like).

Three modelling approximations allowed analytical derivation of a rate expression for the network of Figure 4a. First, reactant solvation was considered to be rapid and in virtual equilibrium at reaction conditions. This is not true during the small heat-up period. Second, solvated reactant molecules were modelled to be caged and thus unable to follow the neat pyrolysis reaction path. Third, the solvated species R^S was considered to exist only at reaction conditions, and ambient analysis by gas chromatography would thus provide the sum $R^* = R + R^S$ as the observable for kinetics analysis.

Eq. 1 is a general rate expression for guaiacol, DBE, BPA and BPS disappearance through the network of Figure 4a; the values of the rate expression parameters will be different for each reactant. For the parameter values listed in Table II, the predictions of Eq. 1 and its integration over time

$$r = \frac{-dR^*}{dt} = \left[\frac{(n+1)k_1}{1 + K_S S^m} + \frac{k_2 S}{(1 + 1/K_S S^m)} \right] R^* \quad 1)$$

are illustrated in Figures 5a and 5b as plots of the reaction rate and conversion, respectively, as a function of S at a fixed temperature and time. Note the predicted minima are quite general and in accord with the experimental observations. The magnitude and occurrence of these minima are clearly dependent upon the values of rate expression parameters.

In the mechanism of Figure 4b the general reactant R fragments directly through either a pyrolysis or solvolysis pathway to product spectrum P_1 or P_2 , respectively. The rate constants k_1 and k_2 of Figure 4b include the activation volume pressure dependence, which was not accounted for in Figure 4a; on the other hand, cage effects and thus solvated reactant R^S are absent in Figure 4b. Qualitatively, the overall disappearance rate and conversion will pass through a minimum in pressure, and thus water density, if k_1 decreases faster than $k_2 S$ with increases in solvent concentration S. Cage effects in Figure 4a and pressure-dependent rate constants in Figure 4b thus account for the same experimentally observed behavior.

SUMMARY AND CONCLUSIONS

The overall reaction of each of guaiacol, DBE, BPA and BPS in dense water is a superposition of neat pyrolysis and solvolysis reaction pathways. Observed product spectra shift from purely pyrolysis-like to solvolysis-like with increases in water concentration. For a given reaction temperature and time, the reactants' conversions pass through relative minima as the water concentration increases. Two mechanistic interpretations provide consistent predictions. The first comprises parallel pyrolysis and solvolysis reaction pathways, the latter occurring through a solvated reactant intermediate to which pyrolysis is denied. The second is a superposition parallel neat pyrolysis and solvolysis pathway with associated rate constants that are pressure dependent.

ACKNOWLEDGMENT

This work was supported by the U.S. DOE under Grant No. DE-FD22-82PC50799 and the USDA Forest Products Laboratory under Grant No. FP-83-0560.

REFERENCES

- (1) Squires, T.G.; Aida, T.; Chen, Y.; Smith, B.F. ACS Div. Fuel Chem. Preprints, 1983, 28, No. 4, 228.
- (2) Simmons, M.B.; Klein, M.T. "Free Radical and Concerted Pathways in Dibenzyl Ether Thermolysis"; Ind. Eng. Chem. Fundam. (accepted for publication 1985).
- (3) Lawson, J.R.; Klein, M.T. "The Influence of Water on Guaiacol Pyrolysis"; Ind. Eng. Chem. Fundam. (accepted for publication 1984).
- (4) Townsend, S.H.; Klein, M.T. "Dibenzyl Ether as a Probe into the Supercritical Fluid Solvent Extraction of Volatiles from Coal with Water"; Fuel (accepted for publication 1985).
- (5) Abraham, M.A.; Klein, M.T. "Pyrolysis of Benzyl Phenyl Amine Neat and with Tetralin, Methanol and Water Solvents," I&EC Prod. Res. and Dev. (accepted for publication 1984).

Table 1
Reaction Conditions

<u>Model Compound</u>	<u>Reactant Concentration</u>	<u>Temperature/°C</u>	<u>Holding Time/min</u>
DBE	1.71	374	15
	1.71	374	45
	1.71	374	60
BPA	0.564	386	5
	0.688	386	20
	0.604	386	30
BPS	0.547	300	10
	0.521	300	20

Table 2
Rate Expression Parameters Used in the Prediction of Figure 5

<u>Parameter</u>	<u>Value</u>
n	1
k ₁	0.06 sec ⁻¹
k _S	1.5 mol ⁻¹
m	1
k ₂	0.3 sec ⁻¹ mol ⁻¹

Figure 1
Influence of Water Density

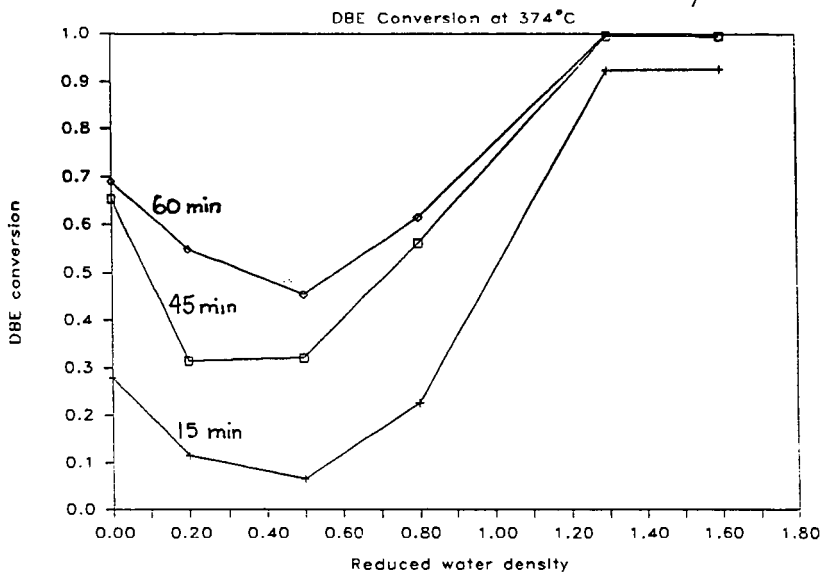


Figure 2
BPA conversion vs. reduced water density
T = 386 C

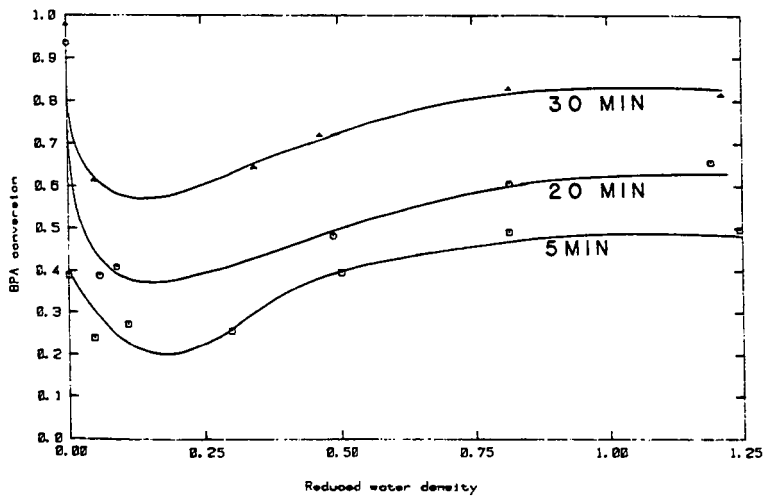


Figure 3
BPS conversion vs. reduced water density
T = 300 C

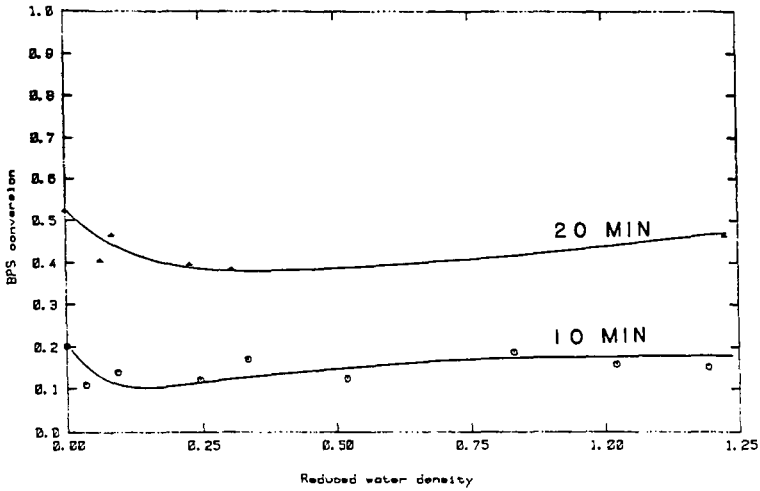


Figure 4: Proposed Reaction Network

Figure 4a: Cage effects

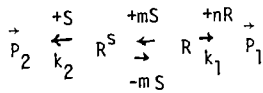


Figure 4b: Pressure-dependent rate constants

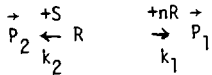


Figure 5A
Predicted reaction rates vs.
reduced solvent density

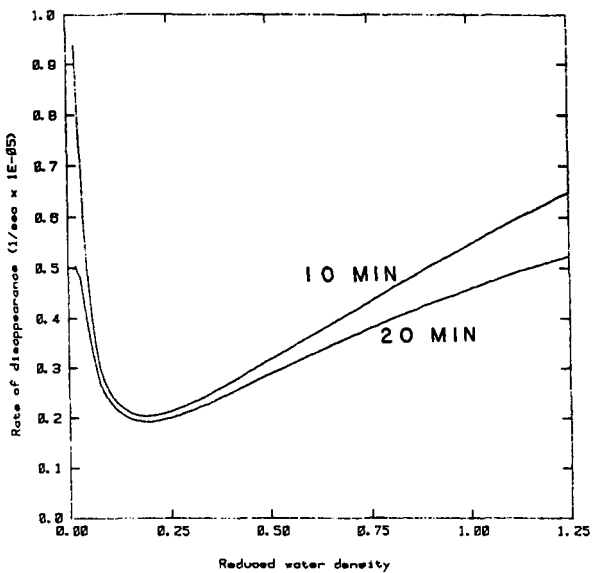
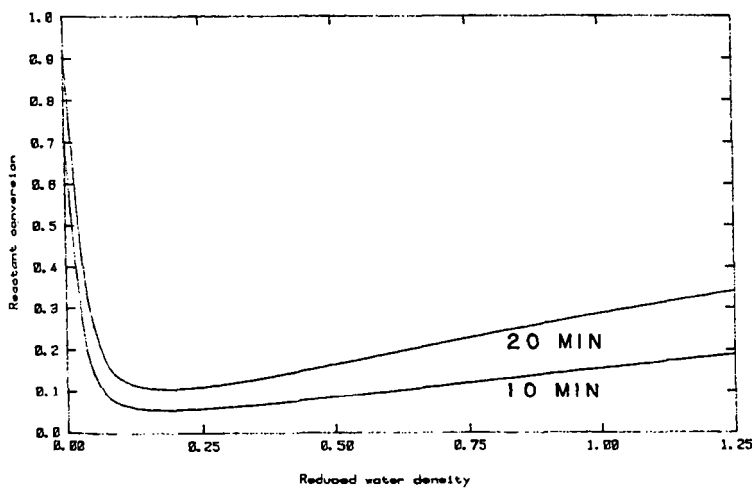


Figure 5B
Predicted conversion vs.
reduced solvent density



Chemical Modelling in the Manipulation of Lignin Pyrolysis Pathways

John B. McDermott, Michael T. Klein and John R. Obst*

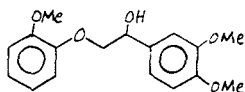
Department of Chemical Engineering, University of Delaware, Newark, DE 19716

*USDA Forest Products Laboratory, Box 5130, Madison WI 53705

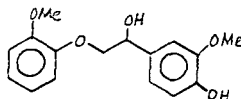
1. Introduction

Lignin is an abundant renewable resource of chemical structure apparently amenable to pyrolytic depolymerization to phenolics. However, the utility of recovered products is low, as only 10-15 wt.% of lignin mass is typically recovered as single-ring phenolics and the major products are gases, char and other high-molecular weight materials.

Chemical modelling provides insight into the intrinsic chemical pathways that superimpose to make observable lignin pyrolysis complex. This use of model compound information can also implicate both the favorable and deleterious reaction pathways that may be susceptible to acceleration or circumvention through catalysis or solvolysis. Along these lines, the three classes of experiments reported herein are of : i) lignin pyrolysis; and thusly derived modification strategies of ii) catalytic dehydrogenation of lignin prior to pyrolysis and iii) solvolytic depolymerization of lignin in supercritical water (SCW). We focus on the reactions of the β -ethers that help link lignin into a polymer, of which the glycols veratrylglycol- β -guaiacyl ether (VGE, structure I) and guaiacylglycol- β -guaiacyl ether (GGE, structure II) are simple models.



I



II

Thermolyses of pine wood, kraft lignin and a milled wood lignin in SCW also permit scrutiny of the relevance of model results to the reactions of real systems.

2. Experimental

Table I summarizes the experiments in terms of the reactants, catalysts and solvents, as well as the associated reaction conditions of temperature, pressure and reactants' concentrations. The reactants VGE and GGE were synthesized as described fully elsewhere (1). The reactor was a 316 stainless steel batch tubing bomb whose construction and use has been described fully elsewhere (2). Product analysis was accomplished by GC and GC-MS, which enabled the calculation of a mass balance index, defined here as the sum of the masses of the product spectra components divided by the initial mass

of substrate charged to the reactor.

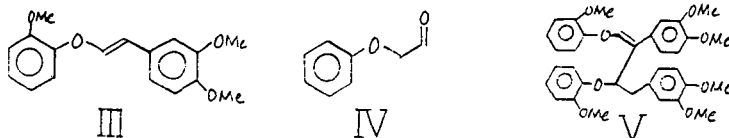
3. Results and Discussion

Results are discussed in two major sections. Within the first, three subsections delineate model compound pyrolysis results, a pyrolysis network, and a brief motivation of the modification strategies, respectively. Within the second major section, subsections present the results and implications of model compound, lignin and whole-wood experiments pertaining to the modification strategies.

3.1. Pyrolysis Results and Implications

3.1.1. Products and Kinetics

VGE. The four major products of VGE pyrolysis were guaiacol, 3,4-dimethoxyacetophenone (3,4-DMA), and cis and trans forms of the vinyl ether III.

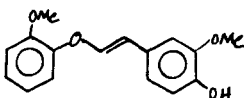


Less abundant products were *o*-cresol, veratrole, 3,4-dihydroxyacetophenone, glycolaldehydeguaicol ether (IV), β -hydroxy-3,4-dimethoxyacetophenone and a dimer of the vinyl ether that had a molecular weight of 572 (such as V).

The temporal variations of both the mass balance and the major products' molar yields are shown in Figure 1 for pyrolysis at 315°C. The mass balance nonclosure became more severe as both reaction temperature and time increased and asymptotically approached an approximate value of 0.4. The positive initial slope of the vinyl ether (both *cis* and *trans* forms) is suggestive of primary product formation. Guaiacol appeared with a smaller but nonzero initial slope and was likely a minor primary product; the large ultimate yields of guaiacol indicate that it was also a significant secondary product. Similarly, 3,4-DMA appeared with a small positive slope that suggests primary product formation.

The variation of the product spectrum with pyrolysis temperature is informative. The only observable products at 250°C were the two forms of the vinyl ether, which were asymptotically stable with time, and trace amounts of guaiacol. At the two intermediate temperatures the vinyl ethers appeared with initial slopes far greater than that for guaiacol and attained maxima in yield before undergoing secondary decomposition. Pyrolysis was so facile at 380°C that the initial slopes of both vinyl ethers and guaiacol could not be determined with precision. Guaiacol yields traversed a maximum at this temperature and its secondary decomposition was to *o*-cresol, phenol and catechol products. It is also interesting to note that the yield of guaiacol was always in excess of the sum of the yields of 3,4-DMA and its likely secondary reaction products acetovanillone and 3,4-dihydroxyacetophenone (DHA).

GGE. The major products of GGE pyrolysis at 250°C were guaiacol and acetovanillone; lesser amounts of cis and trans 1-(3-methoxy-4-hydroxyphenyl)-2-(2-methoxyphenoxy) ethylene (vinyl ether VI) and vinyl-guaiacol.



VI

The temporal variations of the molar yields of the major products and the mass balance are shown in Figure 2. The disappearance rate of GGE far exceeded that of VGE. The mass balance approached an approximate value of 0.4, as was observed for VGE pyrolysis. The initial slopes of guaiacol and acetovanillone formation were both positive, suggesting these to be primary products, although that for guaiacol far exceeded that for acetovanillone. The acetovanillone yield passed through a maximum at approximately 30 min whereas guaiacol appeared to be stable with time. Finally, both forms of the vinyl ether VI appeared to be primary products, whereas vinyl-guaiacol appeared to be the product of a secondary reaction.

3.1.2. Reaction Pathways

The foregoing suggests that VGE pyrolysis comprised the pathways illustrated in Figure 3. Two primary pathways were operative, the major of which being dehydration to the vinyl ethers and the minor being direct fragmentation to guaiacol and, likely, an enol intermediate capable of rapid tautomerization to 3,4-DMA. Each of the primary products was susceptible to secondary reactions. The detection of the dimer of the vinyl ether as well as the progressive nonclosure of observable products' material balance are both indicative of vinyl ether polymerization to species too heavy to elute during GC analyses. Paring of the vinyl ether or its presumed oligomers was also clearly operative. It is noteworthy that the ultimate material balance of 0.4 is closely equal to the weight fraction of the guaiacol moiety in VGE.

Whereas GGE pyrolysis pathways were analogous to those for VGE, the selectivity to each was markedly different: α - β dehydration of GGE was much less significant than its cleavage to guaiacol and acetovanillone. The large yields of guaiacol, far in excess of the acetovanillone yields, indicate secondary guaiacol formation by the cleavage of the guaiacyl group from the vinyl ether VI or any of its subsequent polymers. Of interest is the presence of vinyl-guaiacol, which could be a product of the homolytic cleavage of vinyl ether VI. Its analogue, vinyl-veratrole, was absent from VGE pyrolysis. Acetovanillone was subject to secondary degradation.

3.1.3. Motivation of Catalytic and Solvolytic Modification Strategies

The pyrolysis results detailed above show that a significant β -ether reaction pathway was its undesirable dehydration to a vinyl ether that subsequently underwent yield-reducing polymerization reactions. The ultimate recovery of single-ring products from these substrates could thus be enhanced by reducing the reaction selectivity to the dehydration pathway. Catalytic dehydrogenation of the aliphatic hydroxyls of VGE and GGE to carbonyls would not only prevent the dehydration, and thus circumvent its associated ill effects, but also allow better utilization of the two substrate hydrogen atoms that would otherwise be rejected with the water. For example, shuttling of this hydrogen would allow for the stabilization of free-radicals formed during the subsequent pyrolysis of a dehydrogenated and deoxygenated residue.

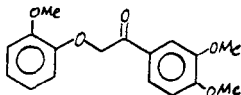
The selectivity of the β -ether reactions may be modified by SCW as well. For example, Lawson and Klein (2) showed that the reaction of guaiacol in SCW was a superposition of parallel pyrolysis and hydrolysis pathways, the selectivity to the latter increasing with increasing water density. The hydrolysis of guaiacol to catechol and methanol was in material balance and the water apparently suppressed a secondary char-forming reaction of catechol. Also, Townsend and Klein (3) showed that the hydrolysis by SCW of DBE to benzyl alcohol competed with the slower pyrolysis of DBE toluene and benzaldehyde. It thus seems reasonable that hydrolysis of the β -ethers by pathways formally similar to those observed for DBE hydrolysis could compete with the formation of the vinyl ethers and circumvent its polymerization. In short, the reactions of guaiacol and DBE in SCW suggest that a suitable modification of the β -ether reaction might be achieved in SCW.

In what follows directly we describe the results of the experiments relevant to both of these strategies

3.2. Modification Strategy-Related Results

3.2.1. Catalytic Dehydrogenation of VGE and GGE

Catalytic dehydrogenation of VGE over $\text{Ni/SiO}_2\text{-Al}_2\text{O}_3$ at 250°C yielded guaiacol, 3,4-DMA, 1-*veratryl*-2-(2-methoxy-phenoxy)-ethanone-1 (the dehydrogenated form of VGE, structure VII), and trace amounts of vinyl ether. The rate of VGE conversion



VII

was roughly threefold higher in the presence of the catalyst than when VGE was pyrolyzed neat.

Figure 4 illustrates the temporal variations of product molar yields for reaction at 250°C . The initial

The variation of methanol yield with water density is illustrated in Figure 7. The addition of external water caused a greater than five-fold increase in the mass yield of methanol over that obtained from neat pyrolysis. The insignificant difference between the yields of methanol observed from pyrolysis at the two highest water densities suggests that both of these pyrolyses were at essentially infinite dilution in water.

For both temperatures examined, the sum of the yields of guaiacol, methyl-guaiacol, catechol and methyl-catechol were only slightly sensitive to water density. However, the yields of these phenolics increased monotonically with time during neat thermolysis. In contrast, the yield of guaiacols traversed relative maxima while the yields of catechols increased or were asymptotically stable during reaction in water. Also, the decay of guaiacols was fastest at the highest reduced water density of 1.6 and their maxima in yield occurred at 10 min, compared to 20 min at the intermediate reduced water of 0.8. In general, the total yields of the four major phenolics increased with temperature with the influence of the water being slightly greater but still small at the higher temperature.

Thus the reaction of kraft lignin in SCW included pyrolysis and solvolysis reaction pathways. The hydrolysis of the aromatic methoxyl groups increased methanol yields and shifted the phenolic product spectrum from guaiacols toward catechols. Interestingly, since the mass yield of methanol of 5-6 wt% was higher than the sum of the mass yields of all of the various phenolics, most of the methanol likely resulted from hydrolysis of the methoxyl groups present in the structural skeleton of lignin. These methoxyl groups would be lost to the char fraction under neat pyrolysis conditions.

Milled-wood Lignin. Pyrolysis of milled-wood lignin neat and in the presence of supercritical water at 383°C yielded methanol, guaiacol, methyl-guaiacol, catechol and methyl-catechol as major products.

The temporal variations of the single-ring products are shown in Figure 8. The positive initial slopes of guaiacol and methyl-guaiacol indicate primary formation of these products. The zero initial slope of catechol and methyl-catechol suggest secondary product formation. The guaiacols traversed maxima at approximately 10 min for reaction both neat and in SCW. The sum of the four major phenolic products increased twofold in the presence of SCW. This is markedly different from the kraft lignin results where no net increase of the phenolics was noted.

Figure 9 shows the temporal variations of the methanol yields parametrically with reduced water density. The initial slopes of the methanol yields indicate primary product formation for all cases. The yields of methanol increased approximately fourfold with the addition of external water. The intermediate density produced virtually the same methanol results as the highest density. This is similar to the kraft lignin results.

Loblolly Pine Wood. Neat pyrolysis of loblolly pine wood at 383°C yielded methanol and guaiacol

slopes of both guaiacol and 3,4-DMA are near zero and thus suggestive of secondary product formation. The 1-veratryl-2-(2-methoxy-phenoxy)-ethanone-1 had a small but positive initial slope and was likely a primary product. All products attained maxima at approximately twenty minutes. The maximum yield of single-ring products (guaiacol and 3,4-DMA) was approximately 0.43, which compares with the 0.06 yield obtained from neat thermolysis at 250°C for 30 minutes. Particularly notable in this enhanced product recovery was the large yield of 3,4-DMA which represents the veratryl portion of the VGE molecule. The initial rate of formation of 3,4-DMA approximately equaled that for guaiacol but the ultimate yields of 3,4-DMA were in excess due to the secondary degradation of guaiacol. This portion of VGE recovered as 3,4-DMA was normally lost to the vinyl polymerization during neat pyrolysis.

Thus catalysis by $\text{Ni/SiO}_2\text{-Al}_2\text{O}_3$ not only effected the desired dehydrogenation but also appeared to crack the resulting keto-ether with hydrogen addition. The net reaction of VGE to guaiacol and 3,4-DMA was thus in hydrogen balance and a selective rearrangement of the hydrogen already present in the substrate.

The catalysis of GGE over $\text{Ni/SiO}_2\text{-Al}_2\text{O}_3$ yielded the same major products as did its pyrolysis: guaiacol, acetovanillone, vinyl-guaiacol and cis and trans forms of vinyl ether VI. However, the rate of GGE reaction was significantly higher than observed during its pyrolysis, as its conversion was essentially 1.0 after a reaction time of only 10 min. This rate also exceeded the rate of VGE catalysis.

The temporal variations of the product molar yields and mass balance are depicted in Figure 5. The mass balance quickly dropped to 0.2. The only product observed in a significant yield was guaiacol, and its initial rate of formation was higher than for GGE pyrolysis. Guaiacol was also subject to a moderate secondary reaction. The rate of formation of vinyl ether VI was approximately equal to that for neat pyrolysis indicating little or no inhibition of the dehydration pathway by the catalyst. A keto-ether analogous to VII, and hence any evidence of a dehydrogenation pathway, was not observed. The presence of the catalyst thus seemed both to enhance the deleterious dehydration and polymerization pathways as well as to promote charring of guaiacol.

3.2.2. Solvolysis in Supercritical Water

Kraft Lignin. The major products of kraft lignin pyrolysis both neat and in water were methanol, guaiacol, methyl-guaiacol, catechol and methyl-catechol. Smaller amounts of phenol and cresols were also detected.

Temporal variations of these major products for reaction at 383°C are shown in Figure 6. The positive initial slopes associated with guaiacol and methyl-guaiacol shown in Figure 6 indicate that these were primary products. Slopes for catechol and methyl-catechol of essentially zero indicate that these were secondary products. The small positive initial slope for methanol suggests that it formed by a primary pathway, although it was likely both a primary and a secondary product.

while reaction in the presence of supercritical water at the same temperature yielded methanol, guaiacol, methyl-guaiacol, catechol and methyl-catechol as major products.

The temporal variations of the single-ring products are shown in Figure 10. The initial slope associated with guaiacol yield from neat pyrolysis was too small to be determined conclusively. However, for reaction in SCW, the initial rate of formation of both guaiacol and methyl-guaiacol was positive and these thus appear to have been primary products. Catechol and methyl-catechol were evidently secondary products. The overall yield of single-ring phenolics increased three-fold with the addition of external water.

The temporal variations of the yield of methanol is shown in Figure 11 for two reduced water densities. The initial slopes indicate primary product formation in both cases. The yield of methanol was virtually unaffected by the addition of water, which is consistent with the isolated lignin experiments. During pyrolysis, the carbohydrate fraction of the wood should lead to significant yields of water capable of hydrolyzing the methoxyl groups present in the lignin. Since the milled-wood lignin results demonstrated the attainment of an asymptotic yield as the external water loading increased, the addition of external water to the wood would prove an insignificant increment to the water originating from the carbohydrate pyrolysis.

4. References

1. Landucci, L. L.; Geddes, S. A.; Kirk, T. K. *Holzforschung* 1981, **35**, 1, 67.
2. Lawson J. R.; Klein, M. T. *Ind. Eng. Chem., Fundam.* 1985, accepted.
3. Townsend, S. H., and Klein, M. T. *Fuel* 1985, accepted.

Table I - Summary of Reactants and Reaction Conditions

Reactant	Loading (mg)*	Catalyst	Solvent	Temperature	Pressure (psia)
VGE	15	--	--	250°C	26
VGE	15	--	--	315°C	29
VGE	15	--	--	335°C	30
VGE	15	--	--	380°C	32
GGE	15	--	--	250°C	26
VGE	15	Ni/SiO ₂ -Al ₂ O ₃	--	250°C	26
GGE	15	Ni/SiO ₂ -Al ₂ O ₃	--	250°C	26
Kraft Lignin	15	--	--	383°C	32
Kraft Lignin	15	--	H ₂ O	383°C	4260
Kraft Lignin	15	--	H ₂ O	383°C	3466
Kraft Lignin	15	--	--	408°C	34
Kraft Lignin	15	--	H ₂ O	408°C	5750
Milled-Wood Lignin	10	--	--	383°C	32
Milled-Wood Lignin	10	--	H ₂ O	383°C	4260
Milled-Wood Lignin	10	--	H ₂ O	383°C	2467
Pine Wood	35	--	--	383°C	32
Pine Wood	35	--	H ₂ O	383°C	4260

*Reactor Volume was 0.589 cm³

VGE PYROLYSIS 315°C

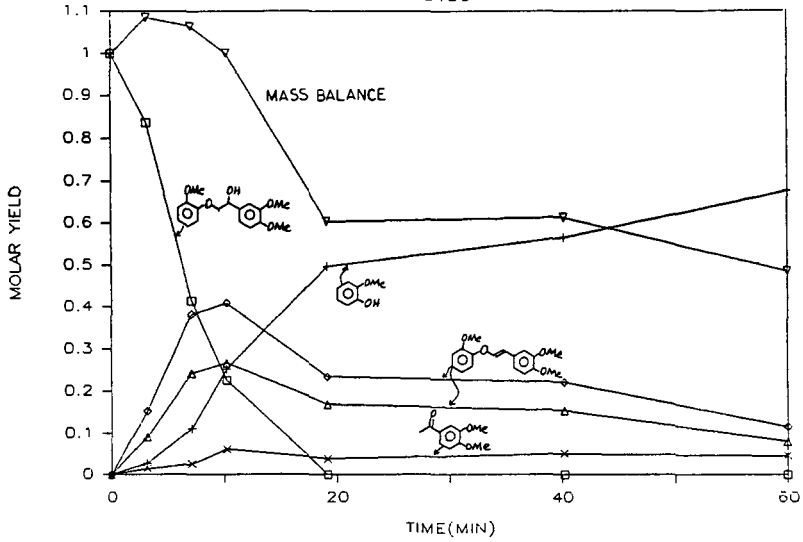


Figure 1. Temporal variations of the yields of the major VGE pyrolysis products at 315°C.

GGE PYROLYSIS 250°C

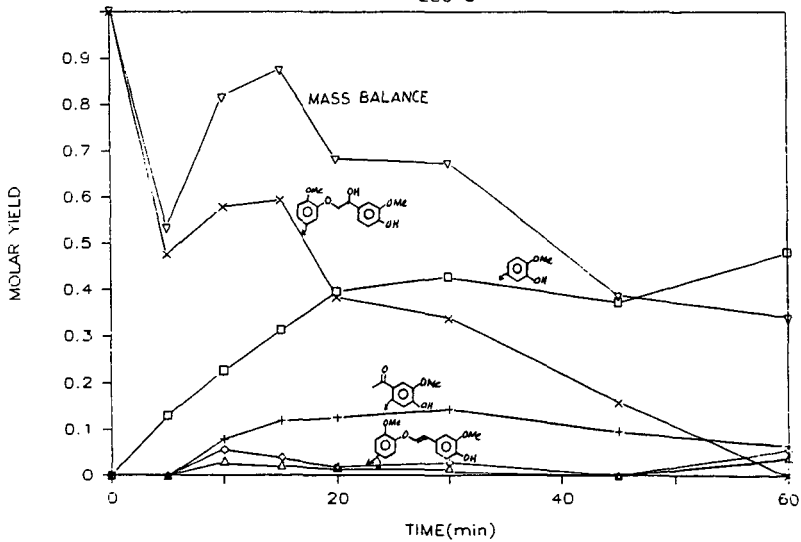


Figure 2. Temporal variations of the yields of the major GGE pyrolysis products at 250°C.

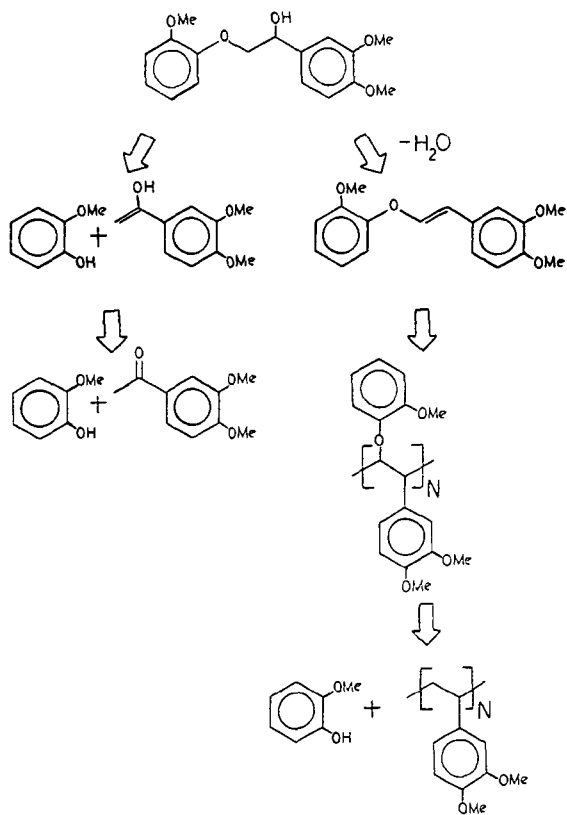


Figure 3. VGE pyrolysis pathways.

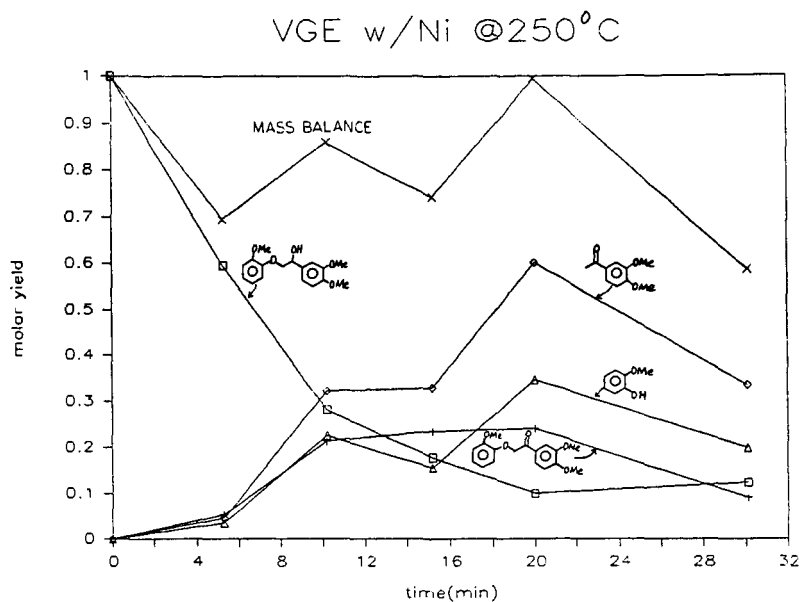


Figure 4. Temporal variations of the yields of the major VGE catalysis products at 250°C.

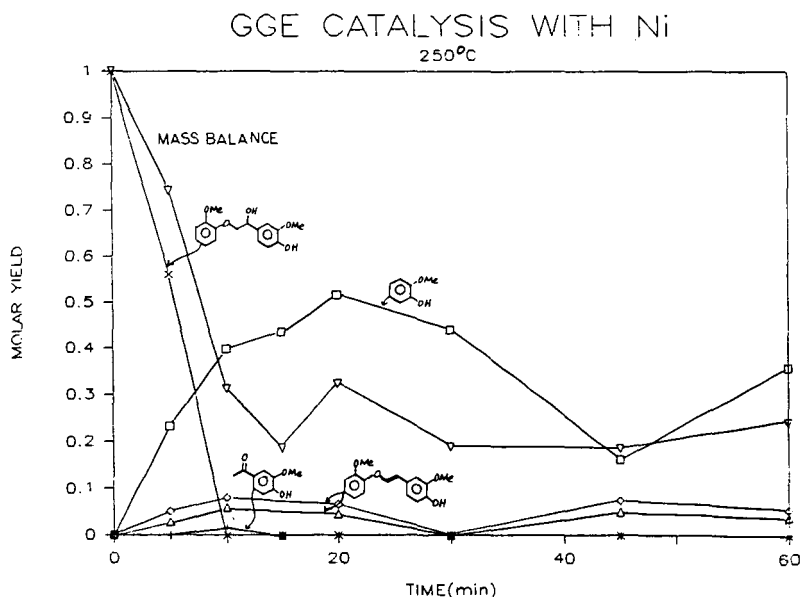


Figure 5. Temporal variations of the yields of the major GGE catalysis products at 250°C.

a) KRAFT LIGNIN PYROLYSIS 383°C
NEAT

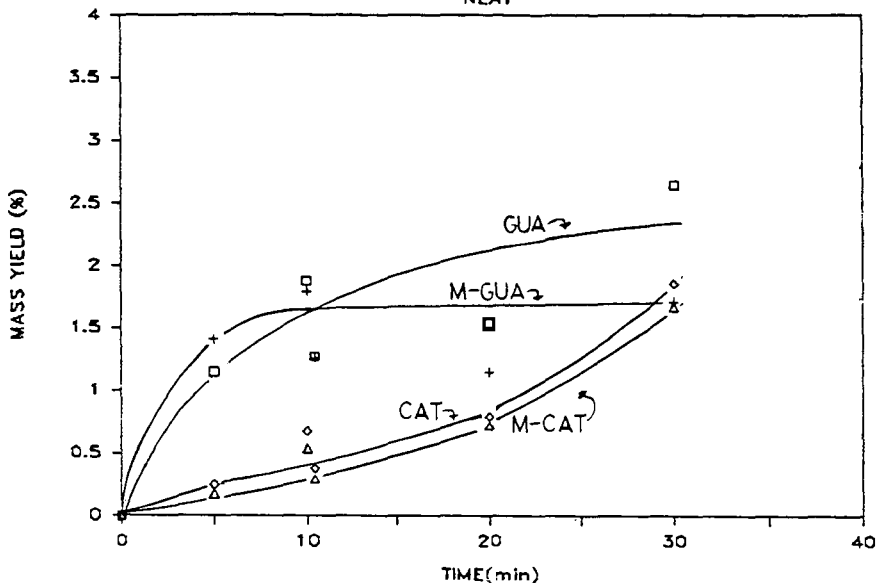
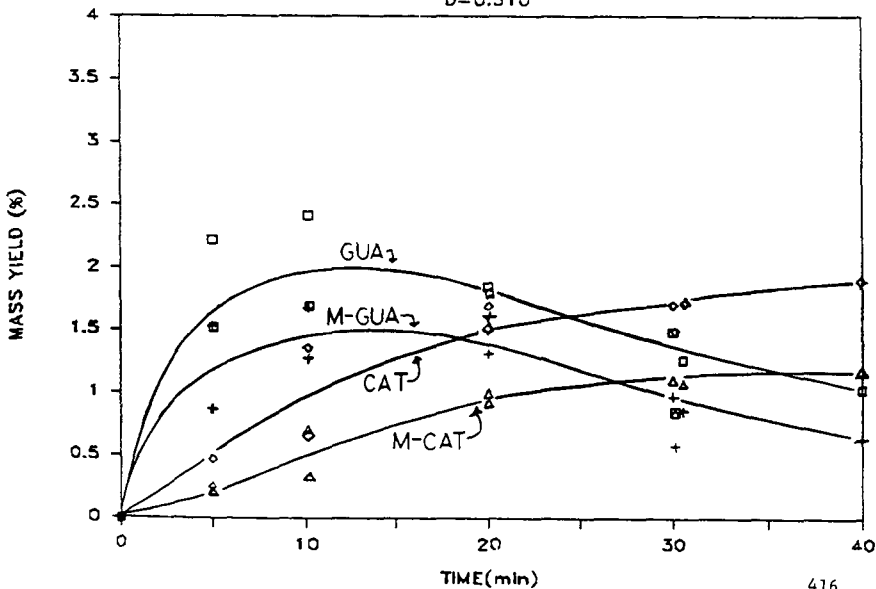


Figure 6. Temporal variations of the yields of the major single-ring products of kraft lignin pyrolysis a) neat b) with water.

b) KRAFT LIGNIN PYROLYSIS 383°C
D=0.510



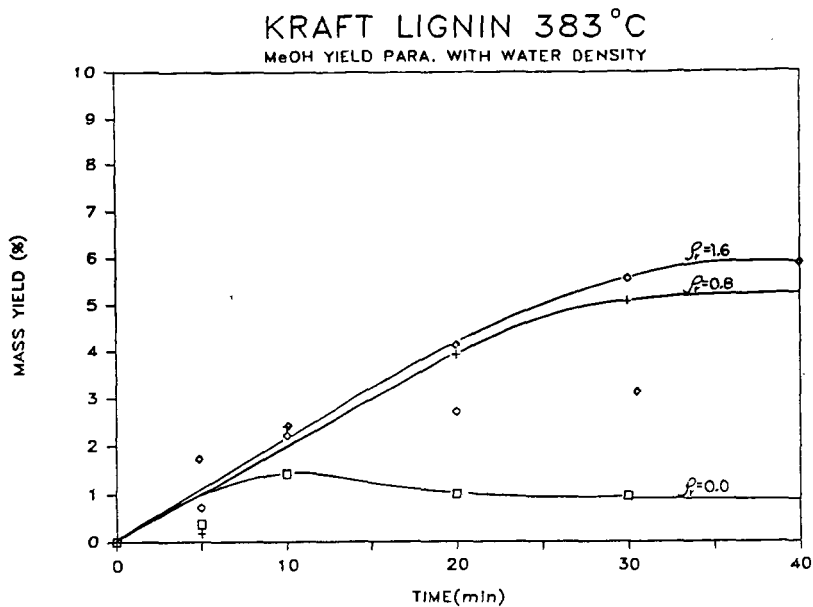


Figure 7. Temporal variation of methanol yield parametric with reduced water density for kraft lignin.

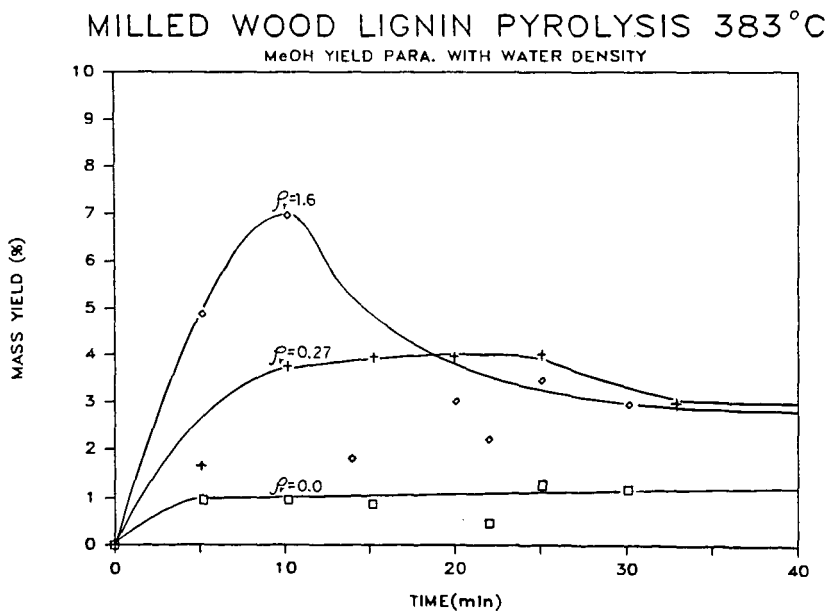


Figure 9. Temporal variation of methanol yield parametric with reduced water density for milled-wood lignin.

a) MILLED WOOD LIGNIN PYROLYSIS 383°C
NEAT

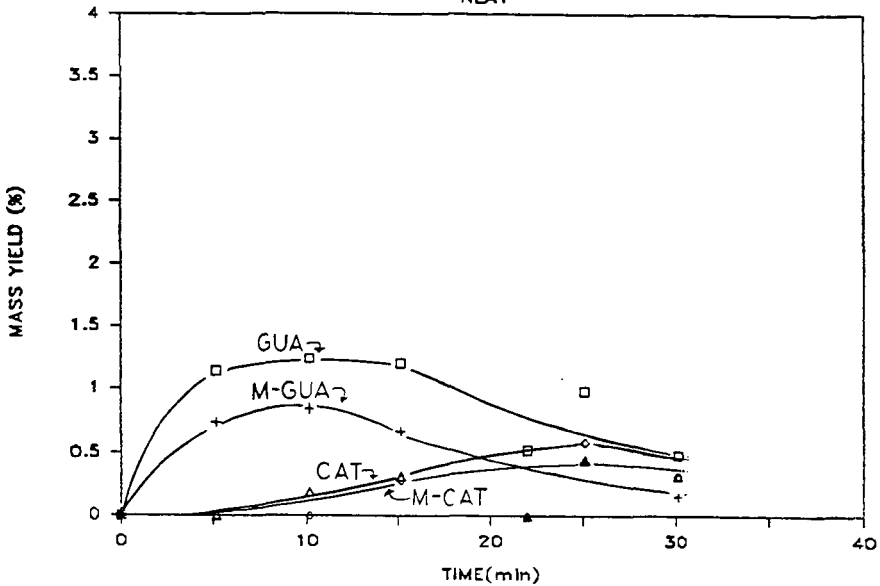
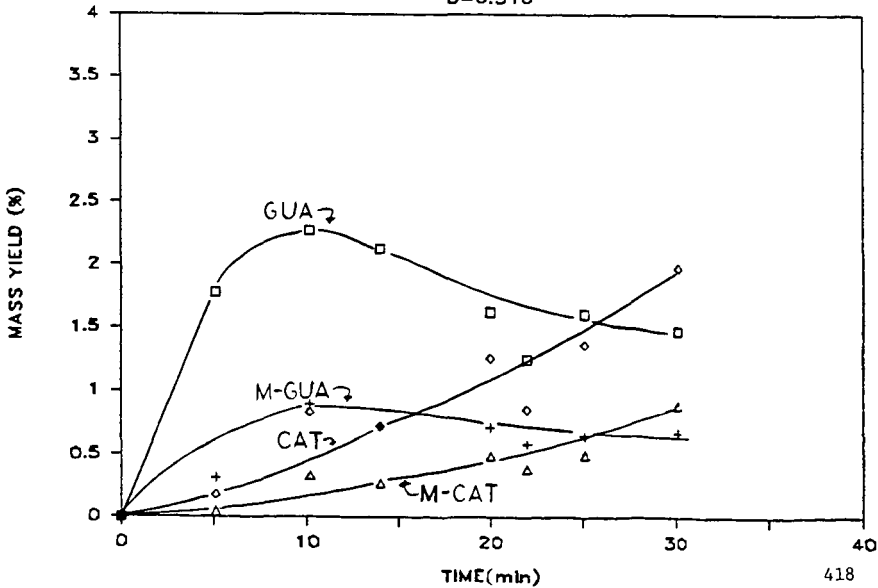


Figure 8. Temporal variations of the yields of major single-ring products of milled-wood lignin pyrolysis a) neat b) with water.

b) MILLED WOOD LIGNIN PYROLYSIS 383°C
D=0.510



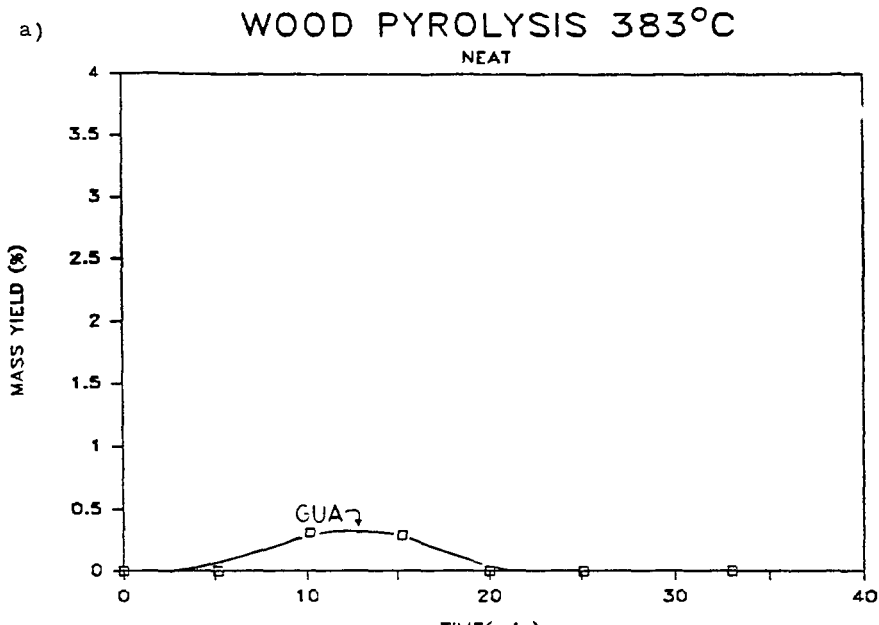
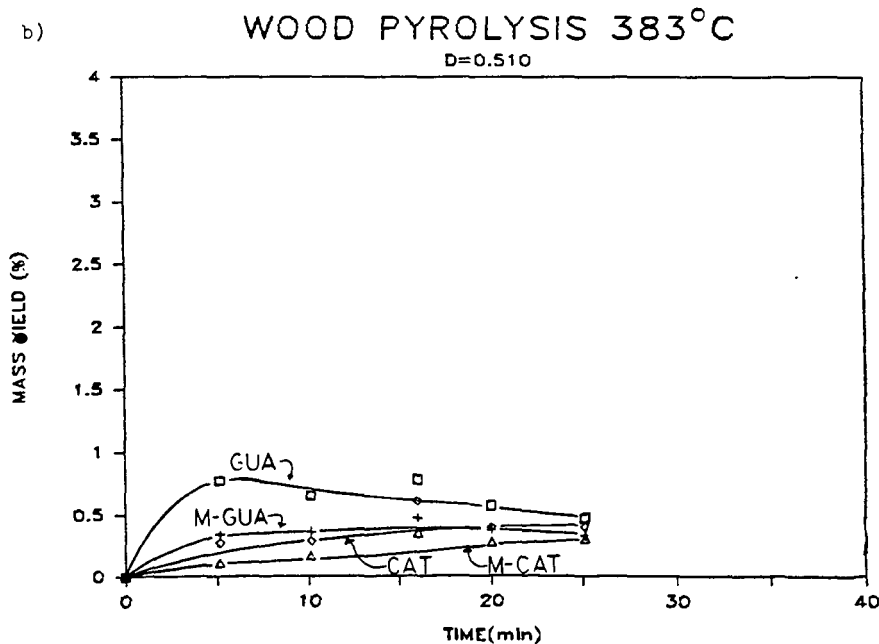


Figure 10. Temporal variations of the yields of the major single-ring products of pine wood pyrolysis a) neat b) with water.



WOOD PYROLYSIS 383°C

MeOH YIELD PARA. WITH WATER DENSITY

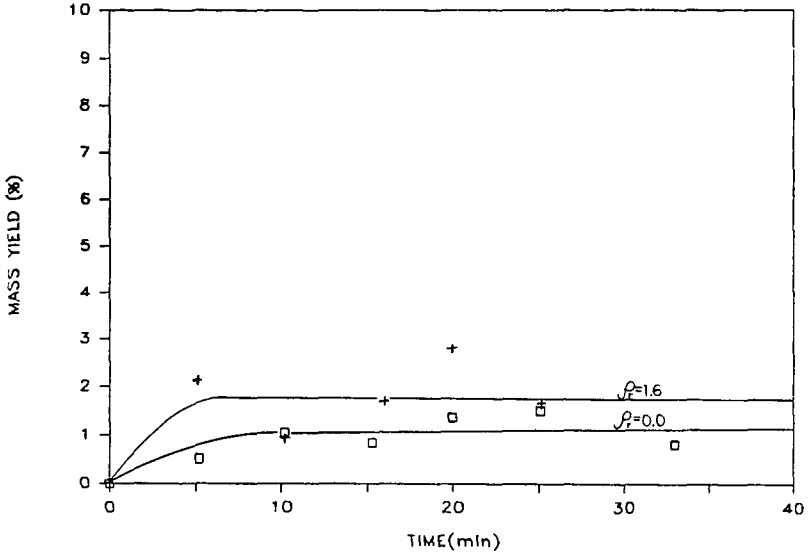


Figure 11. Temporal variation of methanol yield parametric with reduced water density for loblolly pine wood.